# Highlights

## Detecting Harmful Algal Blooms in the Gulf of Maine using a Hybrid Model

Kunal J. Rathore, Jack H. Buckner, James R. Watson

- This paper presents a systematic evaluation of atmospheric-correction processing algorithms for five toxic Harmful Algal Blooms (HABs) taxa detection using Sentinel-3 OLCI observations in the Gulf of Maine.
- Presents a quantitative comparison for added predictive skill gained by incorporating regional ocean model variables into HAB detection framework.
- A demonstration of the value of Imaging FlowCytobots derived, species-resolved in-situ observations for enabling hybrid machine-learning detection across toxic HAB taxa.

# Detecting Harmful Algal Blooms in the Gulf of Maine using a Hybrid Model

Kunal J. Rathore[a], Jack H. Buckner[a] and James R. Watson[a]

[a]College of Earth, Ocean and Atmospheric Sciences, Oregon State University, Corvallis, OR, USA

ARTICLE INFO

*Keywords*:
remote sensing
ocean colors
harmful algae
sentinel-3
machine learning
Imaging FlowCytobot
coastal monitoring
dinoflagellates

ABSTRACT

Harmful algal blooms are a growing threat to marine ecosystems, aquaculture, public health and tourism industries. This study quantifies the value of augmenting simulated outputs of a regional hydrodynamic model with satellite data input to detect harmful algal blooms using machine learning model in Gulf of Maine. And evaluates performance using in-situ Imaging FlowCytobot observations spanning 2018–2025 for five toxin producing algal taxa. Outputs of a regional ocean hydrodynamic model, including sea surface temperature and salinity, were incorporated as predictors with spatio-temporal matched in-situ algal cell concentrations as target labels. Satellite-derived water-leaving reflectances were produced using three atmospheric correction algorithms, enabling systematic comparison of spectral features. ACOLITE atmospheric correction algorithm consistently outperformed OC-SAC and C2RCC in terms of average F1-score across all five taxa. Using hydrodynamic outputs improved detection across three atmospheric correction processes, with F1-score improvements ranging from 2.9% (ACOLITE) to 9.2% (C2RCC); where the best hybrid configuration (ACOLITE + ROMS) achieved average F1-score of 0.745 and provided highest detectability for *Karenia* spp. with F1-score of 0.871. This framework advances operational harmful algal bloom monitoring by demonstrating that atmospheric correction quality and physical oceanographic context act as independent, partially substitutable performance levers for coastal water quality assessment in optically complex nearshore environments.

## 1. Introduction

Harmful algal blooms (HABs) are increasingly in frequency in coastal and open-ocean ecosystems around the world, appear when certain phytoplankton species proliferate and produce toxins, often depleting dissolved oxygen, with severe consequences for marine ecosystems, public health, and coastal economies (Hallegraeff et al., 2021; Anderson et al., 2021). HABs have been reported in coastal waters across all major ocean basins, driven by increasing sea surface temperatures, and increased nutrient runoff (Gobler et al., 2017; Townhill et al., 2018; Pershing et al., 2015). HABs induce substantial economic burden: marine HABs have been estimated to cause an average annual loss exceeding $82 million in the United States through fishery and aquaculture closures, public health expenditures, and disruptions to coastal tourism (Hoagland et al., 2002; Weir et al., 2022; Carias et al., 2024), with inflation-adjusted estimates approaching $100 million per year (Hoagland and Scatasta, 2006; Suddleson and Hoagland, 2021). A recent study estimated loss of $2.7 billion USD to tourism-related businesses during the 2018 Florida red tide bloom (Alvarez et al., 2024). HABs impose measurable health-related costs: a systematic review found that medical treatment, lost income, and reduced well-being from HAB-associated digestive and respiratory illnesses can range from $86 to over $14,600 per case (Jin et al., 2025). Globally, economic damages reach billions of dollars annually, encompassing commercial fishery losses, aquaculture facility closures, monitoring programs, and long-term ecosystem degradation (Hoagland and Scatasta, 2006; Anderson et al., 2021). Looking at a specific region, the Gulf of Maine (GOM) supports shellfish, finfish, and lobster industries which have been repeatedly disrupted by paralytic shellfish poisoning caused by *Alexandrium catenella*, diarrhetic shellfish toxins from *Dinophysis* spp., and by the growing presence of additional toxic HABs (Anderson et al., 2014, 2021). As climate-driven warming continues to change the ocean conditions of this region (specifically Bay of Fundy, that has most of the aquaculture sites) (Pershing et al., 2015), improving monitoring and detection of HAB has become a critical management concern.

*Corresponding author
rathorek@oregonstate.edu (K.J. Rathore)
ORCID(s):

Effective HAB management requires timely, spatially resolved information on bloom occurrence, intensity, and composition, yet such data remain difficult to obtain at operational decision-making scale (Stumpf et al., 2003; Anderson et al., 2021). Traditional monitoring relies on water sampling techniques, which is labor-intensive and produces limited observations due to logistical constraints (Trainer et al., 2020). Nevertheless, early detection is critical key for management actions (shellfish harvest closures, aquaculture facility transport or mitigation, and releasing public health advisories) must be rapidly implemented, before toxin concentrations in harvested organisms exceed regulatory thresholds (Anderson et al., 2021; Trainer et al., 2020). In coastal systems such as the Gulf of Maine, blooms can develop advect over tens of kilometers in days, and even span multiple management jurisdictions simultaneously, adding mitigation challenges (McGillicuddy et al., 2011). Therefore, reliable and low-latency HAB detection capabilities are essential for evidence-based HAB management framework.

Two latest advancements have increased the ability to provide low-latency HAB monitoring in ocean waters. First, the Imaging FlowCytobot (IFCB), an automated submersible flow cytometer that produces high-resolution images of phytoplanktons, which are further categorized to species or genus level using supervised machine-learning algorithms (Olson and Sosik, 2007; Sosik et al., 2020). Deployed at fixed coastal stations and aboard research vessels, IFCB instruments provides observation at better sampling rate then conventional bottle sampling technique, yielding higher temporal and spatial count of observations for both coastal and shelf waters (Olson and Sosik, 2007). WHO HAB Hub data portal (`https://habhub.whoi.edu/`), avails multi-year time series records for derived cell concentrations in the U.S. East Coast – introducing a valuable dataset useful for evaluating data-driven HAB detection models at regional scale. Second, the accessibility to remote sensing-ocean color data has improved the spatial and temporal extent of HAB observations (Stumpf et al., 2003; Hu et al., 2005). Multi- and hyperspectral reflectances provide bloom-relevant optical signals improving HAB detection from earth observations (Hu et al., 2005; Gower et al., 2005, 2008; Lange et al., 2025).

Despite these advances, several challenges remain in using these observations into species-specific HAB detection in ocean water. Reflectance-based indices are act as proxies of algal biomass, not designed to resolve specific algal taxa or discriminate co-occurring taxa using ocean color (OC) optical features (Kudela et al., 2015; Stumpf et al., 2003). Subsequently, retrieval quality varies with the atmospheric correction algorithm (level-2 processing), particularly in high-latitude coastal scenes with low solar elevation, high aerosol loading or land-adjacency effects (Lange et al., 2025). Persistent cloud cover (especially in GOM region) also reduces the count of useful observations. Satellite reflectances only capture the surface water state and do not reveal the subsurface physical and chemical conditions that govern bloom dynamics (McGillicuddy et al., 2011; Anderson et al., 2014).

Previous work by Li et al. (2020) investigated *Alexandrium catenella* bloom event along the coast of Gulf of Maine using a coupled physical-biological model. This work analyzed Medium Resolution Imaging Spectrometer (MERIS) satellite observations alongside a coupled physical-biological (hydrodynamic) numerical model to elucidate the mechanisms driving HAB dynamics, demonstrating how wind-driven circulation and active upward cell swimming work contributes to accumulations. To evaluate how simulated physical and chemical properties from the hydrodynamic ocean model influences HAB predictability, we propose a hybrid modeling approach. This approach augments remote sensing data, with hydrodynamic variable as predictors to the machine learning model.

In addition, machine learning approaches have shown skill in predicting the onset of *Karenia brevis* red tides from satellite ocean color products (Izadi et al., 2021), for identifying the physical and chemical drivers of *Alexandrium catenella* blooms through integration with hydrodynamic simulations (Baek et al., 2021), and in the classification of multiple harmful algal genera from abiotic drivers in Mediterranean coastal waters (Tamvakis et al., 2021); and Cruz et al. (2021) provided a broad review on use of machine learning methods for predicting HABs.

In this study, we evaluate a hybrid detection approach for five HAB taxa in the GOM region, where outputs from a Regional Ocean Model (ROM) simulations, are combined with Sentinel–3 Ocean and Land Colour Instrument (OLCI) data (2018–2025) to predict HABs and evaluate against in-situ IFCB cell concentrations (entire workflow Fig.1). We also assess three atmospheric correction algorithm pipelines– Ocean Color Standard Atmospheric Correction (OC-SAC) (solvo and HYGEOS, 2023; for Copernicus, 2022), C2RCC (Brockmann et al., 2016), and ACOLITE (Vanhellemont and Ruddick, 2021), to extract a comprehensive set of spectral features. These satellite-derived predictors are combined with co-located ROM outputs, and evaluated within a classification framework using cross-validation across IFCB observations. The primary contributions of this work are: (i) systematic assessment of atmospheric correction methods for multi-species HAB detection from Sentinel-3 OLCI in Gulf of Maine region; (ii) a quantitative assessment of the added predictive value of hydrodynamic model's outputs; and (iii) a demonstration

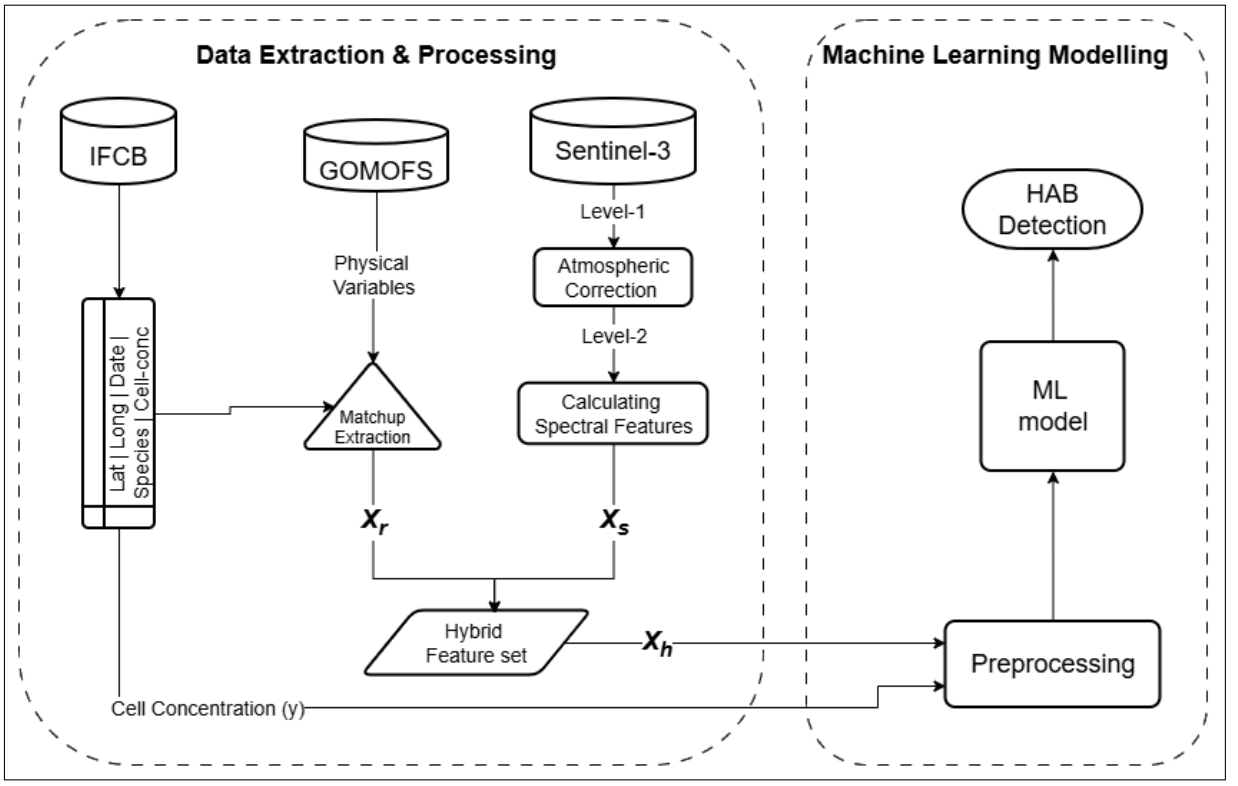


**Figure 1: Overview of the proposed hybrid HAB-detection framework.** In-situ phytoplankton observations are first obtained from the IFCB dashboard for the Gulf of Maine region. For each IFCB sample, temporally and spatially overlapping Sentinel-3 Level-1 scenes are retrieved, and Level-2 processing is performed using three different atmospheric-correction algorithms. From these processed products, a suite of spectral indices are computed corresponding IFCB observation. Physical variables are extracted from the GoMOFS model for matchup locations. Satellite and ROMS-derived features are used as hybrid feature set to train machine-learning model for detecting HAB taxa.

of the utility of IFCB data (spatio-temporal improved in-situ observations) for hybrid machine learning detection across toxic HAB taxa.

## 2. Methods

### 2.1. Study Area

The study area encompasses the Gulf of Maine (GOM), a semi-enclosed marginal sea bounded by the coastlines of Massachusetts, New Hampshire, Maine, and the Canadian provinces of New Brunswick and Nova Scotia (Fig. 2.1). The basin is separated from the North Atlantic by Georges bank and Browns bank, and has depths ranging from 50 m on the banks to more than 300 m in the Jordan and Wilkinson basins (Townsend et al., 2010; Pershing et al., 2015). The sea surface temperatures exhibit strong seasonality, ranging from approximately 2°C in late winter to 20°C in late summer, driven by solar heating and freshwater discharge from major rivers, including the Penobscot, Kennebec, and Merrimack Rivers (Hetland and Signell, 2005). The region is influenced by the cold, nutrient-rich inflow of the Labrador Current through the Northeast Channel and by warmer, more saline slope water from the Gulf Stream, which together produce strong horizontal gradients in water mass properties, nutrient concentrations, and phytoplankton community composition (Pershing et al., 2015; Townsend et al., 2006). Tidal mixing and episodic wind-driven upwelling create localized nutrient enrichment, particularly in coastal embayment and along the western Maine coast, contributing to the region's high biological productivity and susceptibility to harmful algal bloom events (Townsend et al., 2006).

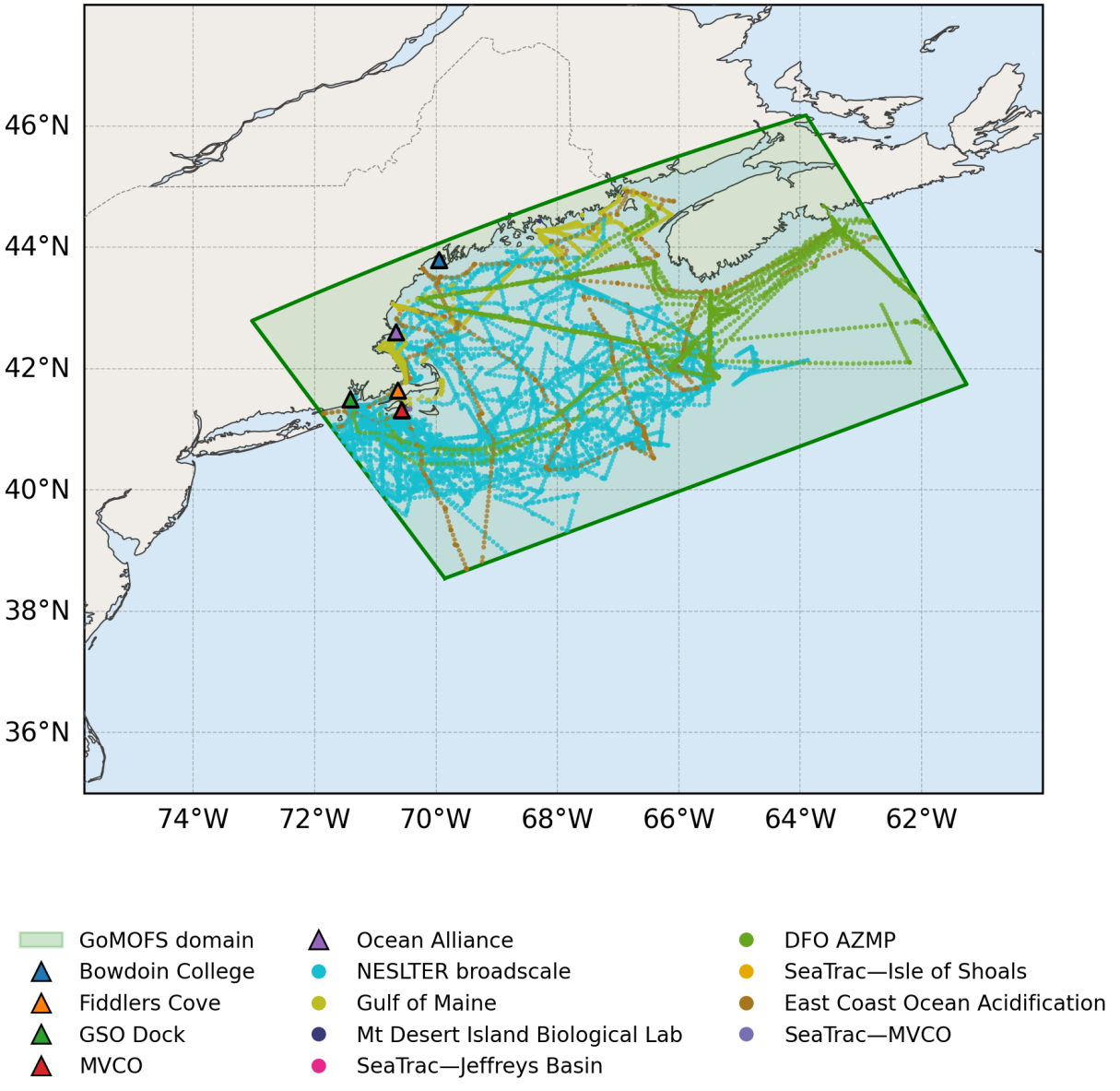


**Figure 2: Study area in-situ monitoring and hydrodynamic model region**. The shaded region bounded by the green line denotes the spatial domain of the Gulf of Maine Operational Forecast System (GoMOFS; Yang et al. 2019), with 700 m surface resolution. Triangles indicate fixed IFCB monitoring stations; Circles represent datasets with relatively sparse sampling, including observations obtained from ship-based platforms, with each point representing sampling location. Station colors correspond to individual datasets as listed in the legend.

The spatial extent of the hydrodynamic model output used in this study is defined by the Gulf of Maine Operational Forecast System (GoMOFS) – a regional ocean model simulation system operated by the National Centers of Environmental Prediction of the National Oceanic and Atmospheric Administration (NOAA) (Yang et al., 2019).

The GoMOFS domain covers the Gulf of Maine and adjacent shelf waters from approximately 41.0°N to 38.5°N and 71.0°W to 61.5°W at a horizontal resolution of approximately 700 m, covering the in-situ monitoring stations used in this study (Fig. 2.1). Satellite and in-situ observations included in the analysis are located within this region, ensuring availability of hydrodynamic model outputs for maximum matching observations.

The Gulf of Maine experiences recurring and economically consequential harmful algal blooms. *Alexandrium catenella* is the primary cause of paralytic shellfish poisoning in the region, with spring bloom events driven by the transport of resting cysts from nearshore sediment sources (Anderson et al., 2014; McGillicuddy et al., 2011). *Dinophysis acuminata* and *D. norvegica* produce diarrhetic shellfish toxins throughout coastal New England (Hattenrath-Lehmann et al., 2013), while *Pseudo-nitzschia* spp., *Karenia* spp. contribute to the region's diverse bloom assemblage. These taxa exhibit distinct optical signatures that makes the GOM a suitable testbed for satellite-based multi-species harmful algal bloom detection (Kudela et al., 2015; Stumpf et al., 2003).

## 2.2. *In-situ* data: Imaging FlowCytobot Observations

In-situ phytoplankton cell concentration data were obtained from the Imaging FlowCytobot (IFCB) (Olson and Sosik, 2007) shared database through the WHOI HAB Hub data portal (`https://habhub.whoi.edu/`) operated by the Woods Hole Oceanographic Institution. IFCB is an automated submersible flow cytometer hat produces high-resolution images of phytoplanktons while submerged in water, these images are further categories into distinct phytoplankton cells at the species or genus level using machine learning algorithm (Sosik and Olson, 2007), finally deriving time series of cell concentrations (cells per Liter) at monitoring stations. We retrieved data for 2018–2025 period which included fixed stations and ship-aboard observations within the GoMOFS region.

Stations with predominantly riverine or estuarine influence (*nauset*, *jamestown*, *lombos*) were excluded to maintain a focus on coastal and shelf waters. For fixed-location stations, instrument coordinates were verified, corrected and in few cases slightly displaced (withing 300m distance) to get meaningful satellite observations in the fjord. Daily cell concentrations were aggregated to the 95th percentile by station and date to characterize bloom-level conditions while reducing the influence of unreasonable outliers. Five HAB taxa in this study have documented shellfish toxicity and human health impacts along the U.S. East Coast: *Alexandrium catenella*, the primary cause of paralytic shellfish poisoning in GOM (Anderson et al., 2014); *Dinophysis acuminata* and *Dinophysis norvegica*, which produce diarrhetic shellfish toxins in coastal New England waters (Hattenrath-Lehmann et al., 2013; Reguera et al., 2014); *Karenia* spp., responsible for neurotoxic shellfish poisoning and fish kills along the U.S. coast and an emerging bloom-forming concern in GOM (Stumpf et al., 2022; Record et al., 2021); and *Pseudo-nitzschia* spp., which produce domoic acid, the causative agent of amnesic shellfish poisoning (Trainer et al., 2012). These five taxa are therefore the focus of the detection framework in this experiment.

## 2.3. Satellite Data

Remote sensing data were acquired from the Ocean and Land Color Instrument (OLCI) aboard the European Space Agency's Sentinel-3A and Sentinel-3B satellites. OLCI provides multi-spectral ocean color observations across 21 spectral bands ($400 - 1020\ nm$) at approximately $300m$ spatial resolution with a near-daily revisit frequency at mid-latitudes (Donlon et al., 2012). Full-resolution Level-1 top-of-atmosphere radiance products (OL_1_EFR) were obtained for study region spanning 2018–2025 period.

To compare the impact of atmospheric correction methods on the satellite-derived ocean color products, three independent processing approaches were implemented. First, Level-2 Water Full Resolution (OL_2_WFR) products were extracted using the sentinel-hub (CDSE) platform, which applies the Ocean Color Standard Atmospheric Correction (OC-SAC) algorithm. OC-SAC uses various processing methods including a neural-network approach trained on radiative transfer simulations, including corrections for Rayleigh scattering, aerosol effects, and gaseous absorption (solvo and HYGEOS, 2023; for Copernicus, 2022). Second, Level-1 satellite products were processed locally using the Case 2 Regional Coast Color (C2RCC) processor (Brockmann et al., 2016) using the European Space Agency provided Sentinel Application Platform (SNAP) (European Space Agency, 2025). C2RCC employs a neural network specifically optimized for optically complex coastal and inland waters. Third, Level-1 data were processed using Atmospheric Correction for OLI 'lite' (ACOLITE) application (Vanhellemont and Ruddick, 2021), a Python-based processing tool that uses dark-spectrum fitting in the near-infrared and shortwave infrared to estimate aerosol optical thickness. ACOLITE was configured with a fixed aerosol optical thickness at 550 $nm$ ($\mathrm{AOT}_{550} = 0.1$) to ensure robust processing during the winter months with low sun angles and frequent cloud cover typical of the Gulf of Maine. Quality control flags from each processor were applied to mask pixels affected by clouds, cloud shadows, land adjacency, and sun glint.

Satellite observations were matched to IFCB cell concentration data using a spatiotemporal window of 2 km radius and $\pm 2$ days, with matchup retained only where at least three valid pixels were available. The spatial window balances the characterization of local optical conditions against the risk of averaging across distinct water masses (Lange et al.,

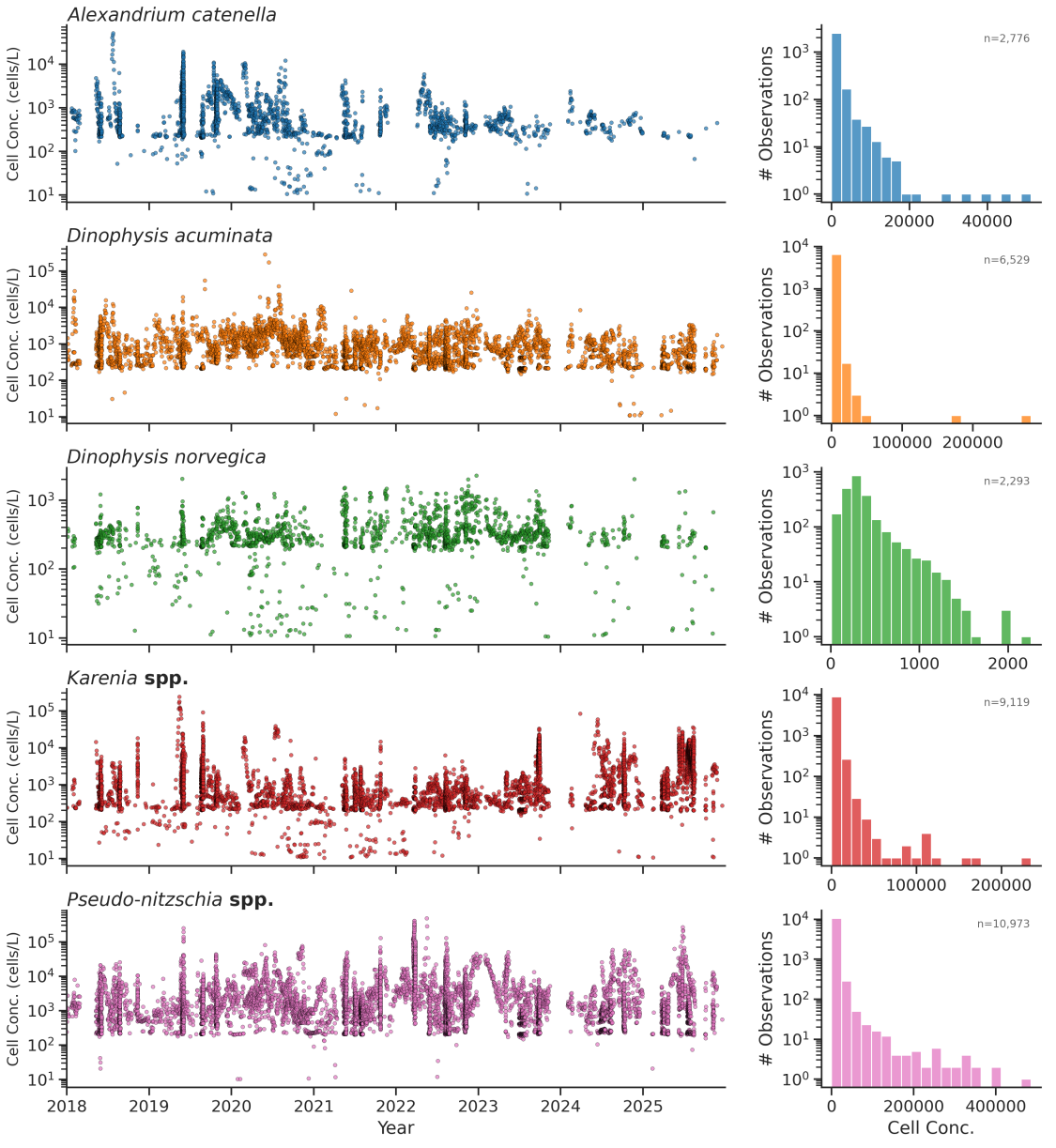


**Figure 3: Temporal dynamics and statistical distributions of harmful algal bloom (HAB) species.** For each of the five HAB species : *Alexandrium catenella*, *Dinophysis acuminata*, *Dinophysis norvegica*, *Karenia* spp., *Pseudo-nitzschia* spp., respectively, the left panels display log-scaled cell-concentration time series (cells/L) spanning 2018–2025, with species labels shown in the upper-left of each subplot. The right panels present the corresponding cell-concentration distributions using histograms, illustrating the frequency and range of observed concentrations for each species.

2025). Within each window, bio-optical indices were computed pixel-by-pixel over Level-2 remote-sensing reflectance ($R_{rs}$), and subsequently spatial aggregation was applied to get median $R_{rs}$ value and median index value across valid pixels. This order of operations preserves the heterogeneity of the bloom-edge that would otherwise be lost by aggregating bands before computing the ratios (Lange et al., 2025).

## 2.4. Ocean Color (OC) Optical features

Remote-sensing reflectance ($R_{rs}$, $sr^{-1}$) is defined as the ratio of water-leaving radiance to downwelling irradiance just above the sea surface, and represents the spectral color of the ocean as observed from space. In visible and near-infrared, $R_{rs}$ is governed by the inherent optical properties of the water column, primarily absorption by chlorophyll-*a* and accessory pigments, scattering by suspended particles, and absorption by water molecules and colored dissolved organic matter (CDOM) (Mobley, 1994). These optical properties create distinct spectral signatures that enable distinction between bloom and non-bloom conditions. Phytoplankton exhibit characteristic absorption near 443 nm (maximum chlorophyll-*a* absorption) and 665 nm (red absorption band), with a reflectance peak near 560 nm and enhanced red-edge reflectance at 700–710 nm during high-biomass conditions. Chlorophyll fluorescence contributes a narrow emission peak near 681 nm that is elevated above the baseline reflectance during bloom events. The band ratio and line-height indices derived from these features provide robust indicators of phytoplankton biomass and bloom intensity that are less sensitive to atmospheric correction uncertainties and CDOM interference than traditional blue-green band ratio algorithms (Gower et al., 2008, 2005; Mishra and Mishra, 2012).

Spectral features were extracted from each atmospheric correction pipeline at nine OLCI bands. Ocean Color indices were calculated pixel-by-pixel within the 2 km spatial window prior to spatial aggregation (Lange et al., 2025), to preserve bloom-edge heterogeneity that would otherwise be lost by aggregating bands before computing ratios. Hereafter, $R_{rs}(\lambda)$ denotes the remote-sensing reflectance at wavelength $\lambda$ (nm), and $\epsilon$ is a small constant ($10^{-10}$) added to the denominators to prevent division to zero.

*Fluorescence Line Height (FLH)* quantifies the chlorophyll-*a* solar-stimulated fluorescence emission peak near 681 nm as its height above a linear baseline connecting flanking bands (Gower et al., 2005, 2008). Because the fluorescence signal is localized to a narrow spectral window and sits above the broader scattering background, FLH is less susceptible to CDOM and sediment interference than blue-green band ratios, making it particularly valuable in the optically complex coastal waters of the Gulf of Maine. Two variants were computed using OLCI bands at 674*nm* and 709*nm* as the baseline anchors:

$$\mathrm{FLH}_{681} = R_{rs}(681) - \left[ R_{rs}(674) + \frac{R_{rs}(709) - R_{rs}(674)}{709 - 674} \times (681 - 674) \right] \tag{1}$$

$$\mathrm{FLH}_{665} = R_{rs}(665) - \left[ R_{rs}(674) + \frac{R_{rs}(709) - R_{rs}(674)}{709 - 674} \times (665 - 674) \right] \tag{2}$$

Their difference, $\mathrm{FLH}_{\max} = \mathrm{FLH}_{681} - \mathrm{FLH}_{665}$, captures the sharpness of the fluorescence peak, which is enhanced during photosynthetically active blooms and forms the basis for the dinoflagellate-specific composite indices (Lange et al., 2025).

*Maximum Chlorophyll Index (MCI).* measures the height of the red-edge reflectance peak at 709nm above a linear baseline between 665 nm and 754 nm (Gower et al., 2005, 2008). During dense surface blooms, strong particle scattering and reduced water absorption elevate reflectance in the 700–710nm regime, producing a red-edge step. MCI is effective in optically complex coastal waters where chlorophyll concentrations exceed 10 $mgm^{-3}$, conditions that can occur during intense surface accumulations of dinoflagellate taxa (Gower et al., 2005; Li et al., 2020):

$$\mathrm{MCI} = R_{rs}(709) - \left[ R_{rs}(665) + \frac{R_{rs}(754) - R_{rs}(665)}{754 - 665} \times (709 - 665) \right] \tag{3}$$

*Green and Blue Line Heights (GLH, BLH)* measures the height of the reflectance spectrum above a linear baseline in the green (490–665 nm, (Eq. 4)) and blue (413–560 nm, (Eq. 5)) spectral windows, respectively (Lange et al., 2025). Dinoflagellates, including *Alexandrium catenella*, tend to exhibit elevated green reflectance relative to diatoms of similar chlorophyll concentration due to differences in pigment packaging and accessory pigment composition, making these line heights useful discriminative traits between taxonomic groups:

$$\mathrm{GLH} = R_{rs}(560) - \left[ R_{rs}(490) + \frac{R_{rs}(665) - R_{rs}(490)}{665 - 490} \times (560 - 490) \right] \tag{4}$$

$$\mathrm{BLH} = R_{rs}(490) - \left[ R_{rs}(413) + \frac{R_{rs}(560) - R_{rs}(413)}{560 - 413} \times (490 - 413) \right] \tag{5}$$

*Dinoflagellate Index (DINI)* normalizes the sharpness of the fluorescence peak ($\mathrm{FLH_{max}}$) by the green spectral signal (GLH) and the blue reflectance, thus amplifying the contrast between active dinoflagellate blooms and phytoplankton assemblages (Eq. 6). DINI has shown to provide reliable *Alexandrium catenella* cell abundance estimates at concentrations exceeding 10,000 cells $\mathrm{L}^{-1}$ ($R^2 = 0.53$) in the Bering and Chukchi sea (Lange et al., 2025):

$$\mathrm{DINI} = \frac{\mathrm{FLHmax}}{\mathrm{GLH} \times R_{rs}(490) + \varepsilon} \tag{6}$$

*Enhanced Bloom Index (EBI)* was introduced as a satellite-based metric to improve detection of phytoplankton blooms in optically complex coastal waters. It incorporates the sharpness of the chlorophyll fluorescence peak together with a blue line-height term, enhancing sensitivity to elevated biomass and fluorescence associated with phytoplankton physiological stress (Tomlinson et al., 2009). EBI has also been shown to detect Alexandrium catenella at concentrations exceeding 3,000 cells $\mathrm{L}^{-1}$ ($R^2 = 0.67$) (Lange et al., 2025).

$$\mathrm{EBI} = \mathrm{FLHmax} \times \mathrm{BLH} \tag{7}$$

*Red Band Difference (RBD)* measures the spectral contrast between the chlorophyll fluorescence peak at 681 nm and the red absorption trough at 665 nm (Amin et al., 2009). Because it operates in the red spectral region, RBD is less affected by CDOM absorption and atmospheric-correction residuals than blue–green indices (Eq. 8). It has been effectively applied to detect blooms dominated by high-fluorescence dinoflagellate species, including *Karenia brevis*.

$$\mathrm{RBD} = R_{rs}(681) - R_{rs}(665) \tag{8}$$

*Normalized Difference Chlorophyll Index (NDCI)* is a normalized ratio that compares the strong chlorophyll-a absorption in the red band (665 nm) with the reflectance peak in the near-infrared (709 nm) (Mishra and Mishra, 2012). Because the ratio is normalized, it's less sensitive to changes in lighting or leftover aerosol effects. NDCI has shown reliable, often strong, relationships with chlorophyll-a concentrations in coastal and estuarine waters, where optical conditions are typically complex (Eq. 9).

$$\mathrm{NDCI} = \frac{R_{rs}(709) - R_{rs}(665)}{R_{rs}(709) + R_{rs}(665) + \varepsilon} \tag{9}$$

*Additional band ratios* were also included to capture broader spectral-shape variation across the visible and near-infrared. *Karenia brevis* Bloom Index (KBBI)– a normalized fluorescence ratio designed to highlight high-fluorescence dinoflagellates (Eq. 10) (Amin et al., 2009). NDNI which captures the difference between the near-infrared red-edge and the blue absorption region, giving it sensitivity across a wide range of biomass levels (Eq. 11). NDWI helps to identify valid open-water pixels by separating them from areas affected by land adjacency or cloud shadow (Eq. 12) (McFEETERS, 1996). The Red-Edge Ratio measures the steepness of the 665–709 nm reflectance rise, which increases with higher chlorophyll concentrations (Eq. 13). GBI combines fluorescence and green-band signals to provide a composite indicator of bloom intensity (Eq. 14).

$$\mathrm{KBBI} = \frac{R_{rs}(681) - R_{rs}(665)}{R_{rs}(681) + R_{rs}(665) + \varepsilon} \tag{10}$$

$$\mathrm{NDNI} = \frac{R_{rs}(709) - R_{rs}(490)}{R_{rs}(709) + R_{rs}(490) + \varepsilon} \tag{11}$$

**Table 1**
Harmful Algal Bloom (HAB) Species Thresholds for Warning and Closure Protocols

| Species | Warning Threshold (cells/L) | Closure Threshold (cells/L) |
|---|---|---|
| *Alexandrium catenella* | 100 | 300 |
| *Dinophysis acuminata* | 200 | 500 |
| *Dinophysis norvegica* | 200 | 500 |
| *Karenia spp.* | 1,000 | 5,000 |
| *Pseudo-nitzschia spp.* | 2,000 | 13,000 |

$$\mathrm{NDWI} = \frac{R_{rs}(560) - R_{rs}(865)}{R_{rs}(560) + R_{rs}(865) + \varepsilon} \tag{12}$$

$$\mathrm{RE} = \frac{R_{rs}(709)}{R_{rs}(665) + \varepsilon} \tag{13}$$

$$\mathrm{GBI} = \mathrm{FLH}_{681} \times \mathrm{GLH} \times 10^6 \tag{14}$$

Simple visible-band ratios (blue/green, green/red, blue/red, red/near-infrared) were also retained to provide a broad spectral shape context representing the full visible spectrum to the machine learning models.

## 2.5. Regional Ocean Model Features

Regional Ocean Modeling System (ROMS) is a hydrodynamic model that solves the hydrostatic, Reynolds-averaged Navier–Stokes equations on a curvilinear grid (Shchepetkin and McWilliams, 2005). It simulates the three-dimensional structure of coastal circulation by representing pressure gradients, tides, river inputs, surface heat and momentum fluxes, and subgrid-scale mixing. Its fine resolution in shallow coastal areas makes it well suited to the stratified, tidally influenced shelf waters of the Gulf of Maine. Simulated variables such as sea-surface temperature (SST) and sea-surface salinity (SSS) capture physical conditions that shape the growth, stratification, and transport of phytoplanktons (Li et al., 2020). SST reflects temperature-dependent growth dynamics for individual HAB taxa, while Salinity reflects the balance between freshwater inputs and offshore water intrusions, both of which shape nutrient supply and stratification patterns relevant to bloom development in Gulf of Maine (McGillicuddy et al., 2011; Townsend et al., 2006).

The hydrodynamic variables in this study were collected from GoMOFS (a NOAA operational ROMS configuration) (Chen et al., 2009) providing nowcast and forecast fields at 700 m horizontal resolution throughout the Gulf of Maine. The model output was accessed via the NOAA's THREDDS data server. For each IFCB observation, the closest same day matchup observations were extracted within a 2 km radius.

## 2.6. Species-Specific HAB Detection via Tree Ensemble Classification

### *2.6.1. Comparative Feature Design*

Two objectives guided the experimental design. The first was to evaluate how much the atmospheric correction methods influences detection skill; the three pipelines (C2RCC, ACOLITE, and the OC-SAC processor) were independently assessed, each producing its own set of spectral characteristics. To ensure a fair comparison, all three pipelines were trained and evaluated on the same set of satellite–IFCB matchup observations, differing only in the spectral feature values derived from atmospheric correction algorithm. The second objective was to evaluate whether augmenting ocean color features with physical variables from hydrodynamic model improves detection performance. To this end, two parallel feature sets were constructed: the ocean color feature set (OC model)–comprising remote-sensing water reflectance and derived bio-optical indices (Section 2.4), and the hybrid feature set (OC+ROMS model)–comprising ocean color features with ROMS-simulated variables (Section 2.5). Both models are trained and evaluated on the identical matchup subset for which valid ROMS output exists, so that the only variable differing between the OC and hybrid models is the composition of the feature set. This design isolates the contribution of the physical context of ROMS from any artifact of sample size (Kapoor and Narayanan, 2023).

### 2.6.2. Target Variable Definition and Bloom Thresholds

Detection was formulated as a binary classification task for each of the five target taxa independently. A matchup was labeled bloom-present when the daily 95th-percentile cell concentration at that station exceeded the species-specific warning threshold (Table 1); otherwise it was labeled bloom-absent. Warning thresholds represent the lowest concentration at which a relevant management authority initiates intensified monitoring or precautionary action, and were preferred over higher closure thresholds because early-stage bloom conditions are where satellite-based detection offers the greatest benefit over conventional monitoring (Anderson et al., 2019; Stumpf et al., 2003).

For *Alexandrium catenella*, the warning threshold of 100 cells $L^{-1}$ follows the Maine Department of Marine Resources action trigger for increased monitoring of shellfish-beds, with closures empirically associated with $\sim$ 300 $cells\ L^{-1}$ (Anderson et al., 2014). For *Dinophysis acuminata* and *Dinophysis norvegica*, the threshold of 200 $cells\ L^{-1}$ reflects the level of consensus of the European Union at which the risk of diarrhetic shellfish poisoning warrants attention to management (Reguera et al., 2014; Blanco and Reguera, 2019). For *Karenia* spp., a warning level of 1,000 $cells\ L^{-1}$ was applied, consistent with the Florida Fish and Wildlife Conservation Commission category boundary above which brevetoxin-related health concerns are recognised (Stumpf et al., 2022). For *Pseudo-nitzschia* spp., a threshold of 2,000 $cells\ L^{-1}$ was adopted based on regional monitoring practice in the Gulf of Maine, where closures are ultimately triggered by shellfish tissue domoic acid measurements rather than cell counts (Trainer and Suddleson, 2005). The corresponding closure thresholds are listed in Table 1 and further details are added to A.1.

### 2.6.3. Random Forest Classifier

Random Forest (Breiman, 2001) was selected as the classification algorithm for several reasons pertinent to this dataset. The method is robust to multicollinearity among features, a property important here because ocean color indices share underlying $R_{rs}$ bands by construction. It requires no prior feature selection and provides embedded permutation-based feature importance estimates, enabling post-hoc interpretation of which spectral and physical variables drive detection skill for each taxon. It is also insensitive to the skewed, zero-inflated cell concentration distributions typical of HAB records (Park et al., 2024). Random Forest has been applied to HAB-related classification and forecasting tasks across multiple regions and taxa: Lange et al. (2025) used ensemble tree methods among other classifiers to detect multiple HAB taxa from Sentinel-3 OLCI in German coastal waters; Medina et al. (2024) used Random Forest with satellite ocean color inputs to forecast *Karenia brevis* blooms along the Florida coast; and Harley et al. (2020) applied Random Forest to classify paralytic shellfish toxin exceedances from environmental variables in Southeast Alaska, demonstrating its utility for threshold-based HAB detection analogous to the approach used here.

A separate classifier was trained for each of the five target taxa, as each species occupies a distinct ecological niche, responds to different physical and optical conditions, and is associated with different toxicological thresholds (Table 1). Combining taxa into a single model would risk masking species-specific signals beneath a shared decision boundary that may not reflect the biology of any individual taxon. To compensate for the low frequency of bloom-present observations relative to bloom-absent observations, class weights were inversely proportional to class frequency during training, ensuring that the minority bloom class contributed proportionally to the learned decision boundary.

### 2.6.4. Model Training and Evaluation

Each classifier was evaluated using repeated train–test splits (80% training, 20% test; $n = 50$ iterations) with binary bloom label. Performance metrics were calculated in the held-out test set at each iteration and summarized as the median and interquartile range across iterations, providing a stable estimate of generalization performance that is less sensitive to any single partition than to a single holdout evaluation. We note that observation counts are unevenly distributed across monitoring stations, with fixed-location sites contributing a larger proportion of the dataset; this imbalance may introduce some station-level influence into the variance of repeated-split estimates.

In total, we evaluated six binary classifier configurations: three atmospheric correction pipelines (ACOLITE, OC-SAC, C2RCC), each trained as a species-specific ocean color (OC) model and a hybrid model (OC+ROMS) with same 9,766 satellite–IFCB matchup observations across 50 repeated experiments. We used two widely used metrics to quantify the performance of the classifiers.

*F1-score* is the harmonic mean of precision–the fraction of predicted bloom events that are confirmed blooms, and recall–the fraction of true bloom events that the classifier detected:

$$F_1 = 2 \cdot \frac{\text{Precision} \times \text{Recall}}{\text{Precision} + \text{Recall}} \tag{15}$$

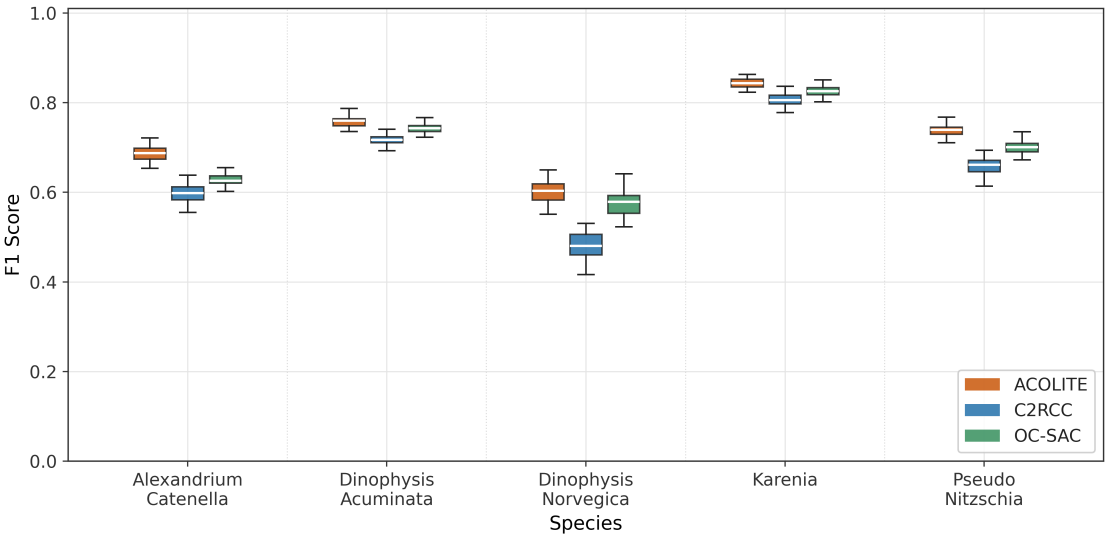


**Figure 4: Performance comparison across HAB species with three atmospheric correction algorithms**. Compares F1-score distributions per species detected at the warning threshold. Boxes show the interquartile range. White lines over box-plot indicates median F-score values and colors indicate atmospheric correction algorithm.

The harmonic mean forces the F1-score to be high only when both precision and recall are high. It penalizes models that achieve high precision by missing many true blooms, or high recall by producing too many false alarms. F1 ranges from 0 to 1 and is well suited for imbalanced datasets because it does not reward correct predictions of the majority class (bloom-absent) (Manning et al., 2008; Saito and Rehmsmeier, 2015). F1-score serves as standard evaluation metric for imbalanced binary classification tasks where both false positives and false negatives carry similar consequences (Manning et al., 2008; Saito and Rehmsmeier, 2015).

*Precision–Recall AUC (PR-AUC)* summarizes classifier performance across all probability thresholds by measuring the area under the precision–recall curve. PR-AUC ranges from 0 to 1, with a baseline equal to the prevalence of bloom-present cases in the dataset (typically far below 0.5 for rare taxa) and a perfect score of 1. Unlike ROC-AUC, PR-AUC is not inflated by the large number of true negatives in rare-event problems, making it a more informative metric when bloom events are infrequent (Davis and Goadrich, 2006; Saito and Rehmsmeier, 2015). Reporting PR-AUC alongside the threshold-specific F1-score allowed performance differences across atmospheric-correction pipelines and feature sets to be compared across the full operating range of each classifier.

## 3. Results

We summarized detection performance using the F1-score and PR-AUC averaged across the five target species. Results primarily focus on warning threshold based models considering operational relevance in regulatory monitoring for HABs (Table 1). Closure-threshold results are provided in the Appendix A.1.

### 3.1. Comparison of Atmospheric Correction Algorithms

Detection skill was consistently highest for ACOLITE, followed by OC-SAC, and lowest for C2RCC across all five species at the warning threshold (Fig. 3; Table 2). Species-level Mann–Whitney U tests confirmed that ACOLITE significantly outperformed both OC-SAC and C2RCC for all five species ($p < 0.001$, large effect sizes throughout), and OC-SAC significantly outperformed C2RCC for all five species ($p < 0.001$, details in Table A.1). The ranking reflects meaningful differences in retrieval quality for the optically complex coastal waters of the Gulf of Maine, where ACOLITE's dark-spectrum fitting in the near-infrared is better suited to high-biomass conditions than the C2RCC neural network trained primarily for open-ocean waters (Vanhellemont and Ruddick, 2021).

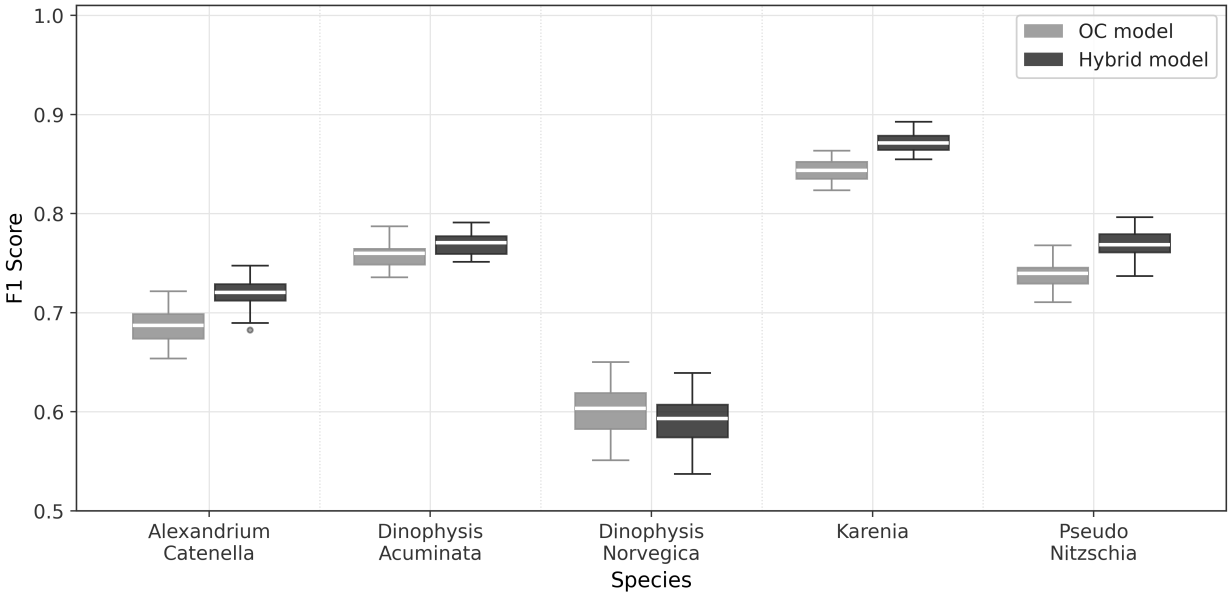


**Figure 5: Performance comparison between Spectral vs hybrid (Spectral + ROMS) features across HAB species with ACOLITE atmospheric correction algorithm**. Compares F1-scores per species detected at the warning threshold. Boxes show the interquartile range. White lines over box-plot indicates median F-score values and colors indicate feature set type for detection.

## 3.2. Ocean Color Model vs. Hybrid Model

Augmenting spectral features with ROMS-derived physical variables improved detection performance for all three atmospheric correction pipelines (Fig. 3.2; Table 2). The improvement was largest for C2RCC, which gained approximately 9.2% in F1-score (0.654 to 0.714) and 7.4% in PR-AUC. OC-SAC improved by approximately 6.0% in F1-score (0.697 to 0.739) and 3.4% in PR-AUC. For ACOLITE, where the OC model already produced the highest baseline performance, the gain was more modest at approximately 2.9% in F1-score (0.725 to 0.746) and 1.7% in PR-AUC. The magnitude of the ROMS benefit was inversely related to OC model performance, consistent with the interpretation that physical context is most informative when spectral retrievals are more uncertain.

Notably, the advantage of ACOLITE over OC-SAC narrowed in the hybrid configuration: *Dinophysis acuminata* ($p = 0.953$) and *Dinophysis norvegica* ($p = 0.801$) became statistically indistinguishable between the two processors, while the remaining three species retained significant but reduced differences. This partial convergence suggests that ROMS-derived physical context compensates for some, but not all, of the retrieval quality difference between the two processors.

Species-level Mann–Whitney tests confirmed that these gains were statistically significant for the large majority of species across all pipelines. For C2RCC and OC-SAC, the hybrid model significantly outperformed the OC model for all five species ($p < 0.001$ for C2RCC throughout; $p \leq 0.006$ for OC-SAC). For ACOLITE, significant improvements were observed for four of the five species ($p < 0.001$).

The exception across all three pipelines was *Dinophysis norvegica*. For ACOLITE, the hybrid model produced no significant change in either F1-score ($p = 0.126$) or PR-AUC ($p = 0.136$) for this species, with marginally negative deltas in both metrics. For OC-SAC, F1-score improved modestly and significantly ($p = 0.006$), but PR-AUC did not ($p = 0.123$). Only for C2RCC did the hybrid model improve both F1-score and PR-AUC significantly ($p < 0.001$). This inconsistency across pipelines likely reflects the thin-layer, subsurface distribution of *Dinophysis norvegica*, whose association with the surface physical gradients captured by GoMOFS is less consistent than for the other target species, and whose detection benefit from physical context appears contingent on the baseline quality of spectral retrievals.

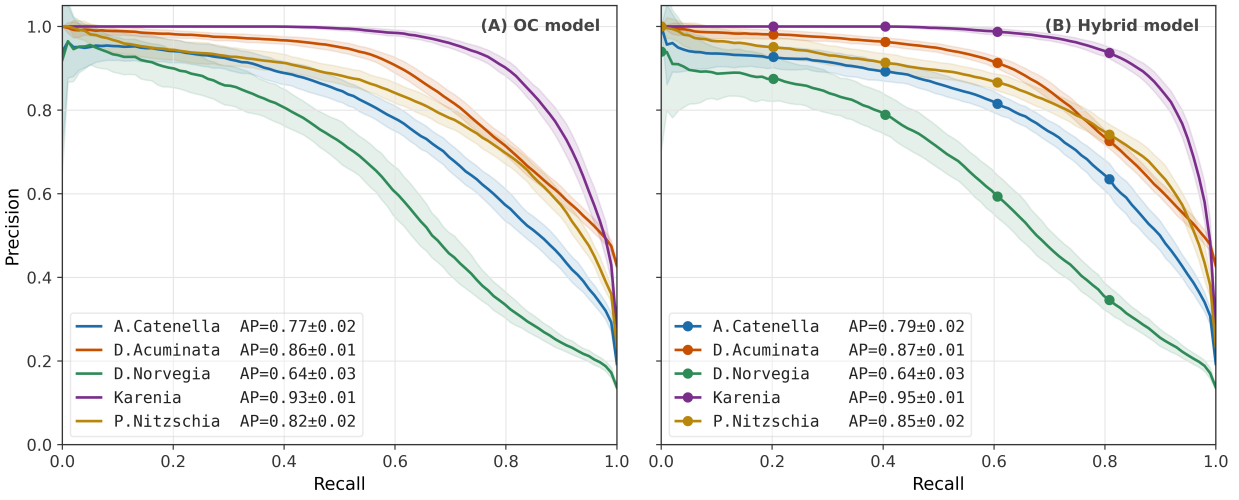


**Figure 6: Precision-Recall Curve comparison across HAB species with ACOLITE atmospheric correction algorithm**. Shows mean precision-recall curves per species for ACOLITE at the warning threshold, averaged across 50 cross-validation folds. Shaded bands indicate ± one standard deviation. Legend entries show mean average precision (AP ± SD).

**Table 2**
Detection performance of OC and hybrid (OC+ROMS) models at the warning threshold. Values are medians across 50 repeated random experiments ($n$ = 9,766 matchups). F1-score are averaged across the five target species in the last row.

| | ACOLITE | | OC-SAC | | C2RCC | |
|---|---|---|---|---|---|---|
| **HAB Species** | **OC** | **Hybrid** | **OC** | **Hybrid** | **OC** | **Hybrid** |
| *Alexandrium catenella* | 0.687 | 0.720 | 0.626 | 0.707 | 0.598 | 0.691 |
| *Dinophysis acuminata* | 0.760 | 0.771 | 0.743 | 0.771 | 0.717 | 0.768 |
| *Dinophysis norvegica* | 0.603 | 0.593 | 0.579 | 0.592 | 0.480 | 0.522 |
| *Karenia spp.* | 0.844 | 0.871 | 0.826 | 0.867 | 0.806 | 0.864 |
| *Pseudo-nitzschia* | 0.740 | 0.769 | 0.701 | 0.760 | 0.662 | 0.729 |
| **Average** | **0.727** | **0.745** | **0.695** | **0.739** | **0.653** | **0.715** |

## 3.3. Species-Specific Performance

Precision–recall curves for all species under the best-performing configuration (ACOLITE hybrid model, warning threshold) are shown in Fig. 6. Species-level performance was heterogeneous. *Karenia* spp. and *Dinophysis acuminata* achieved the highest PR-AUC values, indicating reliable probabilistic discrimination across a wide range of operating thresholds. *Alexandrium catenella* and *Pseudo-nitzschia* spp. occupied an intermediate range, consistent with the diversity of bloom magnitudes and optical conditions under which these taxa occur in the Gulf of Maine. *Dinophysis norvegica* showed the lowest PR-AUC, reflecting the inherent difficulty of detecting a species whose bloom signature is largely obscured from passive surface-sensing instruments (see Appendix **??** for full species-level metrics across all configurations).

For most species, adding ROMS features produced a consistent upward shift in the precision–recall curve relative to the OC model, indicating improved classifier confidence at equivalent recall levels. For *Dinophysis acuminata*, however, the OC and hybrid model curves overlapped across most of the recall range (Fig. 6), consistent with the finding that the ACOLITE spectral feature set already captures the dominant predictive signal for this taxon and that the marginal contribution of physical context is limited.

We also trained regression models to estimate bloom concentration followed a similar pattern to the bloom classifiers. ACOLITE again outperformed OC-SAC and C2RCC across all taxa (Fig. A.3), with *Karenia* spp. showing the highest cell concentration estimates ($R^2 = 0.65$). Adding hydrodynamic predictors improved regression

performance across most taxa (Fig. A.3), with the largest gains for *Karenia* spp. and *Pseudo-nitzschia* spp., consistent with the role of physical conditions in driving bloom intensity for these taxa (Medina et al., 2024; Trainer and Suddleson, 2005).

Similarly, we tested the hybrid model separately for coastal and open ocean observations (Appendix A.2, Fig. A.2). Detection performance was relatively higher in coastal waters, with *Dinophysis acuminata* reaching a median F1-score of 0.85 and observation types – consistent with the near-shore, nutrient-rich conditions that favor *Dinophysis* bloom formation in the Gulf of Maine (Reguera et al., 2014). In open ocean observations, *Karenia* spp. showed the strongest detection skill (median F1 = 0.905), likely reflecting its association with offshore warm-water circulation features that are captured more clearly by both satellite retrievals and ROMS surface fields in cleaner, less optically complex waters (Medina et al., 2024). Among atmospheric correction approaches, ACOLITE outperformed OC-SAC and C2RCC in coastal waters, while all three performed similarly in open ocean conditions, consistent with the fact that ACOLITE was being designed for high-back-scattering coastal environments (Vanhellemont and Ruddick, 2021).

## 4. Discussion

This study addressed two problems: quantify and compare the effect of atmospheric correction process on HAB detection skill, and whether augmenting the hydrodynamic model outputs with ocean color indices improves the detection of HABs. Six model setups: three atmospheric correction approaches (ACOLITE, OC-SAC, C2RCC), for each ocean color model and a hybrid model were evaluated with 9,766 IFCB observations across five toxin producing HAB taxa. Results show that ACOLITE algorithm consistently outperformed OC-SAC, which outperformed C2RCC, with average F1-score improvement of relatively 2.5% to 9.5% between across atmospheric correction processes, confirming that the intermediate processing is a primary determinant of detection skill. Augmenting ocean color indices with hydrodynamic outputs improved detection across all three correction processes, with gains inversely related to ocean color model performance that is, largest for C2RCC (+9.5%) and smallest for ACOLITE (+2.5%), indicating that the physical properties are more informative where satellite retrievals carry higher uncertainty. The best hybrid model setup (ACOLITE + ROMS, F1-score = 0.745) outperformed alternative ocean color model setups, confirming that the quality of atmospheric correction and the physical context contribute independently.

Although the C2RCC algorithm was originally developed for optically complex coastal waters (Brockmann et al., 2016; Doerffer and Schiller, 2007), its neural-network training range may not fully encompass the extreme high-biomass conditions characteristic of HAB events. In Gulf of Maine region, our analysis shows that C2RCC-derived water-leaving reflectance retrievals under-perform relative to dark-spectrum fitting approach such as ACOLITE (Vanhellemont and Ruddick, 2021). This difference is consistent with ACOLITE's empirical estimation of aerosol optical thickness from near-infrared bands, which can make it more resilient when elevated near-infrared water-leaving radiance during bloom conditions biases traditional aerosol retrievals (Vanhellemont and Ruddick, 2021). Meanwhile, the performance gap between ACOLITE and OC-SAC narrowed under the hybrid model setup, as both processed predictors detected *Dinophysis* species with similar skill, suggesting that ROMS physical variables can partially compensate for retrieval-quality differences. This has practical implications for monitoring systems using OC-SAC (which is distributed as a standard Level-2 product): integrating a regional ocean model output can recover much of the performance gap relative to ACOLITE, without requiring a custom atmospheric correction process. However, the gap persisted for other three HAB taxa: including *Alexandrium catenella* (OC-SAC hybrid F1=0.707 versus ACOLITE hybrid F1=0.720), suggesting that the value of dedicated atmospheric correction reprocessing depends on the operational context and the economic cost of missed detections.

HAB dynamics in the Gulf of Maine are governed by physical processes – stratification, advection, and freshwater inputs, that ocean color cannot observe directly (McGillicuddy et al., 2011; Townsend et al., 2006). This is reflected in our results, where the benefit of augmenting hydrodynamic outputs was greatest for the atmospheric correction approaches with the weakest spectral retrievals. The sea surface temperature and salinity served as proxies for water mass characteristics and stratification state, while the lagged features at $\pm 2$ days capture the physical preconditions preceding bloom development that satellite imagery often misses due to cloud cover. Previous work supports this role for physical variables: McGillicuddy et al. (2011) showed that the transport of *Alexandrium fundyense* blooms in the Gulf of Maine is primarily controlled by physical circulation; similarly Medina et al. (2024) demonstrated that physical and hydrodynamic predictors such as current, sea surface temperature, sea level, riverine discharges and nitrogen concentrations significantly improved *Karenia brevis* forecast skill; and Harley et al. (2020) found that temperature, salinity, and wind stress are among the most important predictors for paralytic shellfish toxin

exceedance in Southeast Alaska. Our hybrid framework is operationally different from existing and approach like fully coupled physical–biological model He et al. (2008); McGillicuddy et al. (2011). The presented approach requires no biological sub-model, no bloom trajectory assumptions, and adds minimal computational overhead via nearest-grid-point extraction, making it straightforward to integrate into existing satellite processing pipelines where a regional ocean model simulation outputs are available.

*Dinophysis norvegica* was the only algae taxon for which the hybrid model showed a minimal improvements in detection performance relative to the ocean color model. Further diagnostics with permutation importance provides a partial explanation in this context. While both the detection models (OC and hybrid) primarily relied on broad-spectrum green-wavelength indices (GLH; blue-to-green ratio), salinity and current direction were secondary predictors in hybrid model (Figure A.3). In fact, hybrid model preferred hydrodynamic output features in most of the taxa except *Dinophysis norvegica* and *Karenia* spp. detection. A plausible explanation is that: *Dinophysis norvegica* accumulates in thin layers at the base of the seasonal thermocline (Reguera et al., 2014), which makes it challenging for surface-based satellite and ROMS products to detect the optical and physical characteristics associated with this taxon. Surface salinity and currents may correlate with *Dinophysis norvegica* occurrence in some scenarios but not consistently, introducing noise rather than predictive signal. Sub-surface ROMS variables for example: mixed layer depth, vertical density gradient, near-bottom temperature – which are available from the GoMOFS model but were not included here, may better capture the stratification conditions associated with thin-layer formation for this taxon.

The best-performing model setup (ACOLITE hybrid, F1 = 0.745) offers meaningful improvement over ocean color model (ACOLITE OC, F1 = 0.727) and outperforms C2RCC, which many operational systems currently rely on. For shellfish aquaculture operators and state managers in the Gulf of Maine, where *Alexandrium catenella* closures generate substantial annual economic losses (Anderson et al., 2014), the primary value of a hybrid classifier is spatial coverage: the trained model can be applied to any location within the ROMS domain where satellite retrievals are valid, complementing the geographically sparse IFCB network. Both data streams are freely available at operational latency Sentinel-3 OLCI near-daily and ROMS nowcast four times daily making this approach compatible with near-real-time monitoring workflows in a way that fully coupled physical–biological models may not, given simplicity to train and deploy a machine learning model, reducing calibration and requirements for parameterization burden (McGillicuddy et al., 2011). Lange et al. (2025) used Sentinel-3 OLCI to detect HAB taxa in the Bering and Chukchi seas using remote sensing reflectances and spectral indices; the presented results suggest using hydrodynamic model outputs would likely benefit detection in this case as well.

We acknowledge a few limitations in this work. Training data was derived from a monitoring network concentrated along the western Gulf of Maine coast, and performance at under-sampled or offshore locations is uncertain. The $\pm 2$ day temporal matchup window introduces mismatch uncertainty for rapidly evolving blooms, a limitation shared by satellite-based HAB detection approaches broadly (Stumpf et al., 2003). In this study, hydrodynamic model outputs were restricted to surface variables, limiting representation of three-dimensional processes relevant for subsurface-forming taxa. We also note that this study identified harmful algal taxon and not the toxins levels, and the approach acts as a indicative measurement for harmful conditions and not the the precise toxin conditions. Future work should incorporate sub-surface ROMS variables and bio-geochemical fields (nutrients, mixed layer depth) to address the *Dinophysis norvegica* gap and potentially improve skill for nutrient-sensitive taxa such as *Pseudo-nitzschia* spp. (Trainer and Suddleson, 2005). Extension of the spatial domain to the broader Northeast US Shelf and integration with ROMS forecast rather fields can enable the framework for near-real-time operational early-warning capability.

This study demonstrated that using ocean hydrodynamic model derived variables with ocean color indices from Sentinel-3 improves multi-taxa HAB detection in the Gulf of Maine, with additional gains from using an atmospheric correction approach optimized for complex coastal water. The best model setup (ACOLITE + ROMS) achieved a median F1-score of 0.745 across five HAB taxa at the regulatory warning threshold. Atmospheric correction quality and simulated physical characteristic act as independent and partially substitutable performance levers, a finding of significant relevance to operational management and monitoring programs. The approach is taxon-agnostic, computationally lightweight, and built entirely on freely available operational data, making it a practical framework to sparse in-situ monitoring networks for near-real-time coastal HAB surveillance.

## Acknowledgments

Sentinel-3 OLCI Level-1 and Level-2 data were accessed through the Copernicus Data Space Ecosystem (CDSE), which provided cloud processing resources and open access to pre-processed Level-2 Earth observation products (D. Kovács et al., 2026).

In-situ phytoplankton cell concentration data were obtained from the HABHub Data Portal operated by the Woods Hole Oceanographic Institution (WHOI HABHub Data Portal, 2026), whose open-access distribution of Imaging FlowCytobot observations made this study possible.

## Declarations

- Funding
- We declare no conflict of interest.
- Data availability at (for Copernicus, 2022)
- Code available at `https://github.com/kjrathore/HAB_detection.git`
- Author contribution
  - **Kunal J. Rathore**: Conceptualization, Methodology, Writing – Original Draft, Formal Analysis, Software, Data Curation, Visualization
  - **Jack H. Buckner**: Validation, Investigation, Writing – Review & Editing, Supervision
  - **James R. Watson**: Resources, Writing – Review & Editing, Project Administration, Funding Acquisition

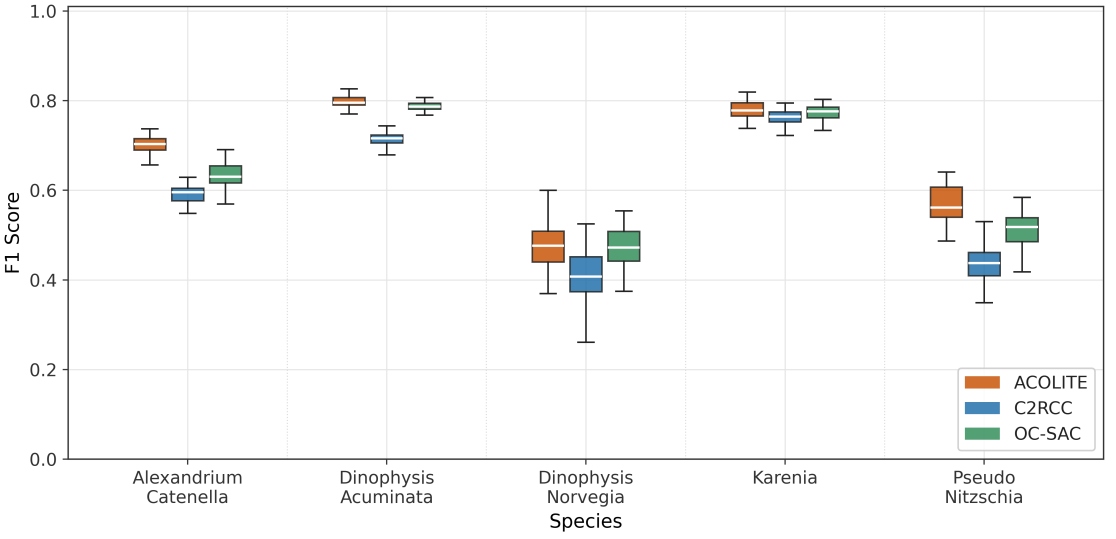


**Figure A.1: Closure threshold based detection performance comparison between atmospheric correction algorithms** from OC model. Compares F1-score (vertical-axis) per species (horizontal-axis) detected. White lines over box-plot indicates median F-score values and colors indicate atmospheric correction algorithm.

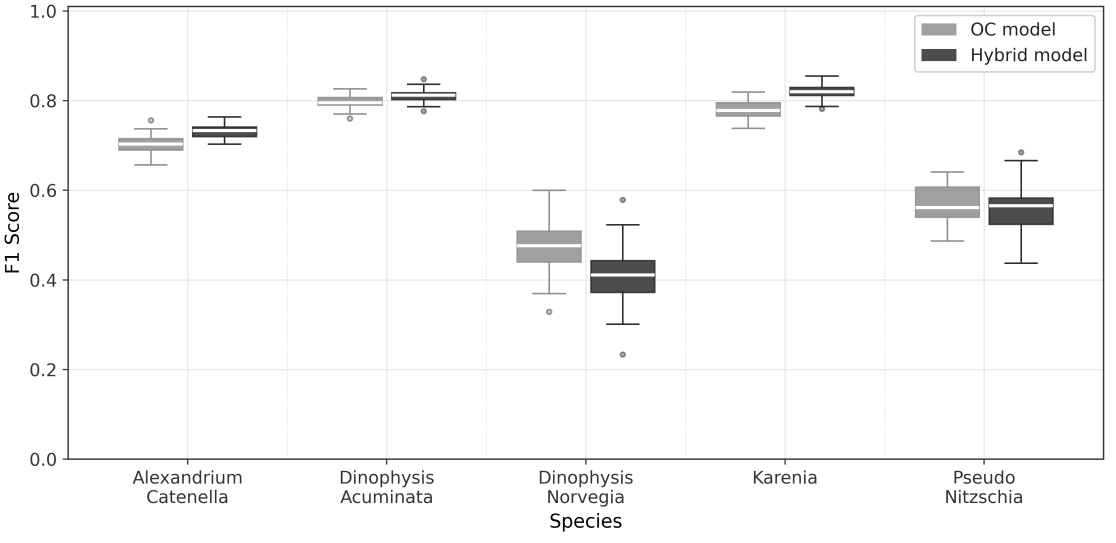


**Figure A.2: Closure threshold based detection performance comparison between optical characteristic vs hybrid model using ACOLITE atmospheric correction algorithm predictors**. Boxes show the interquartile range. White lines over box-plot indicates median F-score values and colors indicate model type for detection.

# A. Appendix

## A.1. Closure threshold results

1. we also eventuated models for closure based thresholds to identify the operational scale of hybrid model. Warning threshold can act as early warning signals whereas closure based model could allow management agencies to prevent human exposure to HAB effect areas precisely and timely. 2. Hence the closure based modeling approach and evaluations are considered in this experiment. 3. Models prepared for closure based detection thresholds indicate again ACOLITE outperforms alternative atmospheric processing algorithms. And hybrid model again shows relatively better detection capability for HAB species except for *Dinophysis norvegica*.

**Table A.1**
Detailed detection performance from OC and hybrid model with different Atmospheric correction procedures. Presented F1-scores and PR-AUC values are the median values over five HAB taxa. Bold values indicate relatively higher performance

| Atmospheric Correction | Model | Threshold | F1-score | PR-AUC |
|---|---|---|---|---|
| ACOLITE | OC | Warning | 0.72487 | 0.80509 |
| ACOLITE | Hybrid | Warning | **0.74613** | 0.81895 |
| OC-SAC | OC | Warning | 0.69729 | 0.78820 |
| OC-SAC | Hybrid | Warning | **0.73934** | **0.81538** |
| C2RCC | OC | Warning | 0.65353 | 0.73778 |
| C2RCC | Hybrid | Warning | **0.71393** | **0.79204** |
| ACOLITE | OC | Closure | 0.66529 | 0.71440 |
| ACOLITE | Hybrid | Closure | **0.66572** | **0.74803** |
| OC-SAC | OC | Closure | 0.63746 | 0.69451 |
| OC-SAC | Hybrid | Closure | **0.66066** | **0.74959** |
| C2RCC | OC | Closure | 0.58183 | 0.63760 |
| C2RCC | Hybrid | Closure | **0.62184** | **0.70608** |

## A.2. Near-shore versus open ocean detection analysis

Prepared data was split into coastal and open ocean groups based on observation location and dataset names (provided in HAB-Hub data). Observations from fixed stations located either in fjords or within $5km$ of the coastline – were classified as coastal; the rest as open ocean (includes NESLTER broadscale, AZMP, Gulf of Maine). The model was trained on all observations regardless of location; only the test set was split by group to examine how detection performance varied across the two settings

## A.3. Regression analysis

In addition to the binary classifiers, we trained regression models to estimate bloom intensity for observations where cell concentrations exceeded the species warning threshold (Table 1). The regression target was $\log_{10}(\text{cells/L} + 1)$, and HistGradientBoosting regressor (a variant of Gradient Boosting algorithm) was trained separately for each HAB taxa. The same six model types used for classification (three atmospheric correction approaches, each with and without ROMS features) were evaluated here. The regression was trained and tested only on observations where cell concentrations exceeded the species warning threshold, as estimating bloom intensity below this level is not meaningful.

We evaluated performance using train-test (80/20 split) cross-validation (80/20 split) with 50 runs, reporting mean $R^2$-score on the log scale and RMSE in back-transformed cells/L. We report cross-validation performance is the reported estimate. Feature importance was computed using permutation importance on the last cross-validation fold.

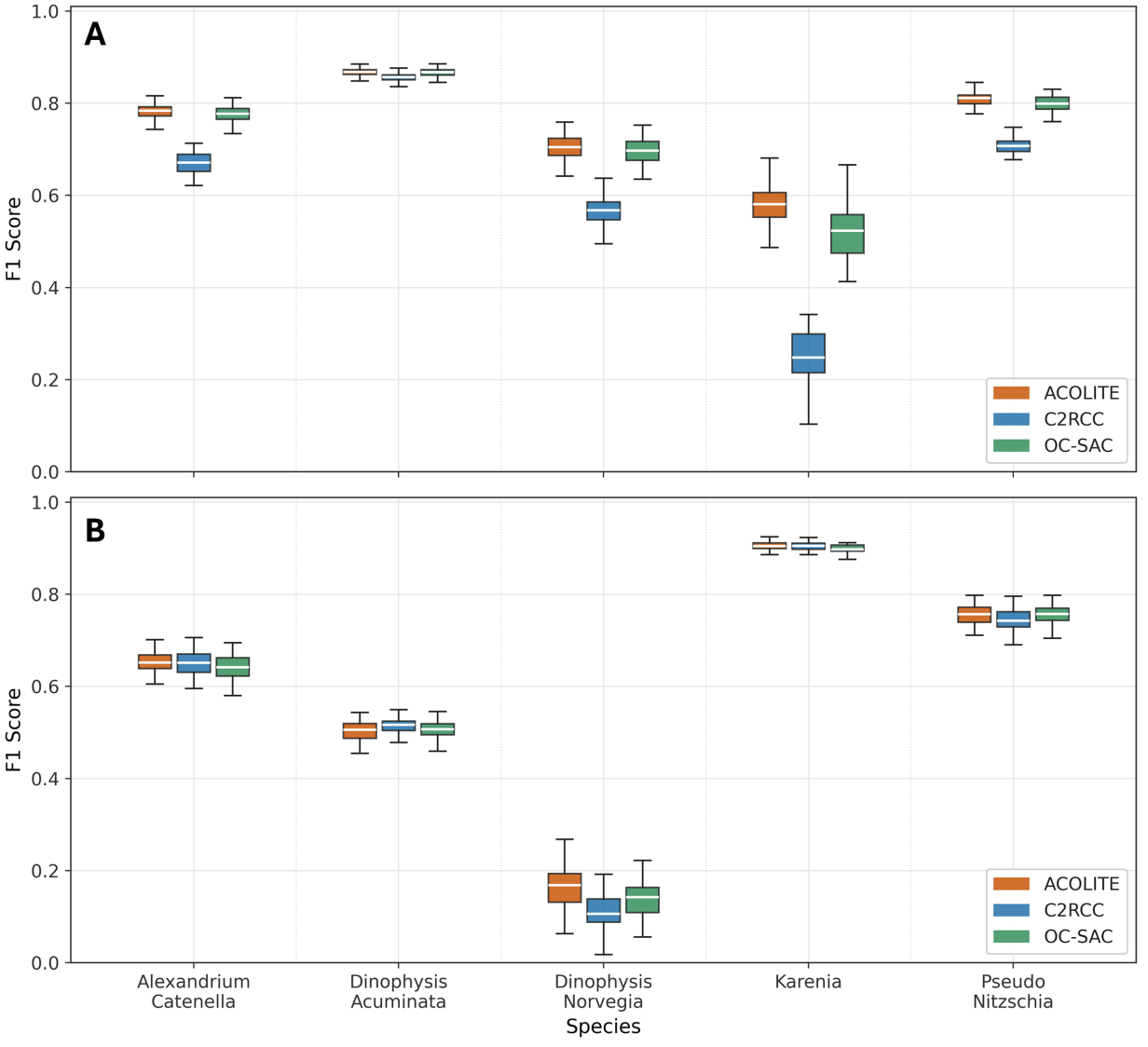


**Figure A.3: Performance comparison across HAB species with three atmospheric correction algorithms**. Compares F1-scores per species detected at the warning threshold with hyrbid model predictions. Panel A: Performance with fixed location (mostly coastal) observation; Panel B: Performance with Ship-based observations (open ocean water). Boxes show the interquartile range. White lines over boxplot indicates median F1-score values and colors indicate atmospheric correction algorithm.

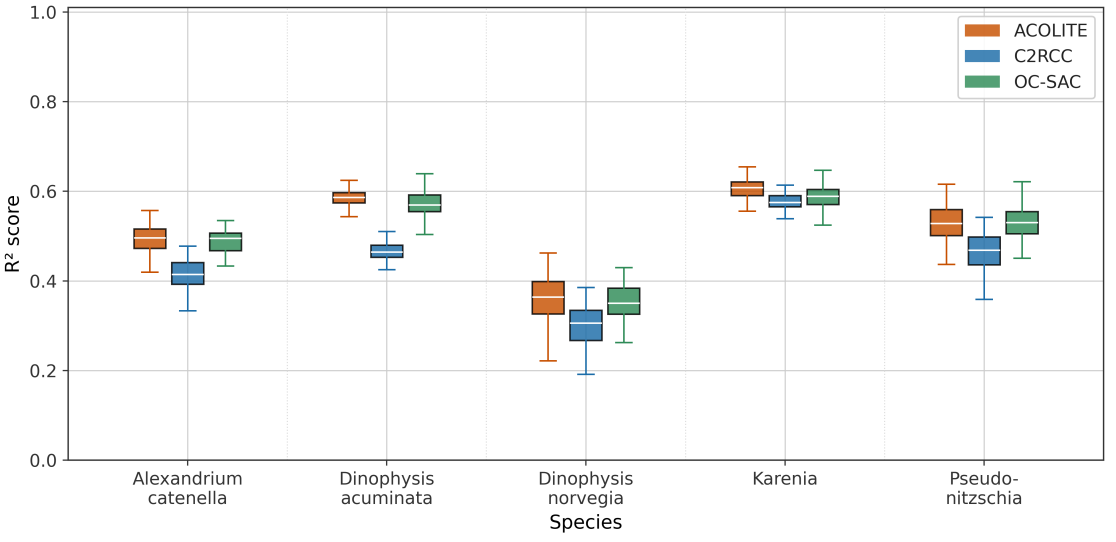


**Figure A.4: Regression performance comparison between atmospheric correction algorithms to quantify bloom intensity** from hybrid model. Compares $R^2$-score (vertical-axis) per species (horizontal-axis). White lines over box-plot indicates median F-score values and colors indicate atmospheric correction algorithm.

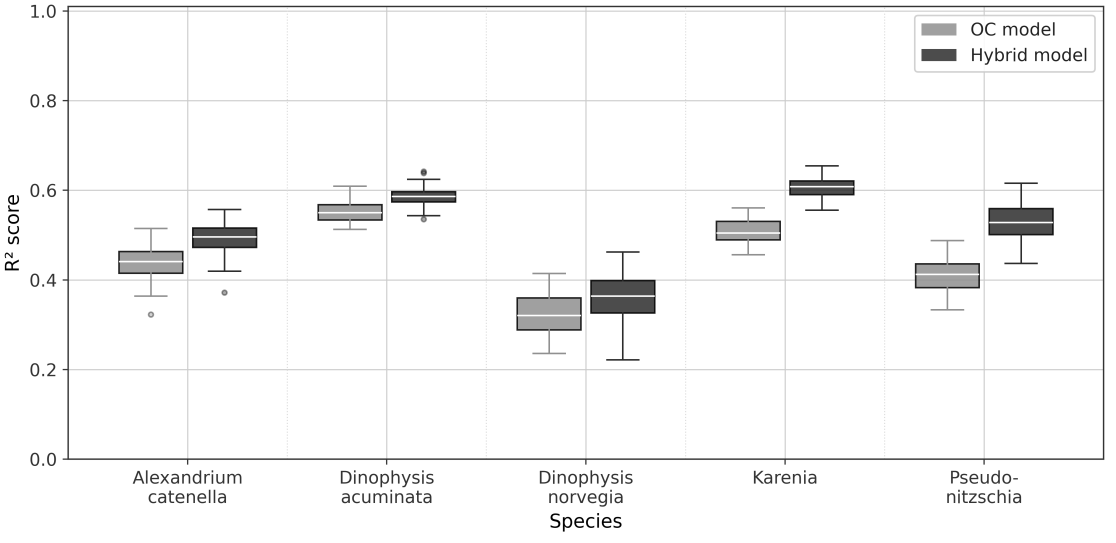


**Figure A.5: Regression performance comparison between optical characteristic vs hybrid model using ACOLITE atmospheric correction algorithm predictors**. Compares $R^2$-score (vertical-axis) per species (horizontal-axis). Boxes show the interquartile range. White lines over box-plot indicates median F-score values and colors indicate model type for detection.

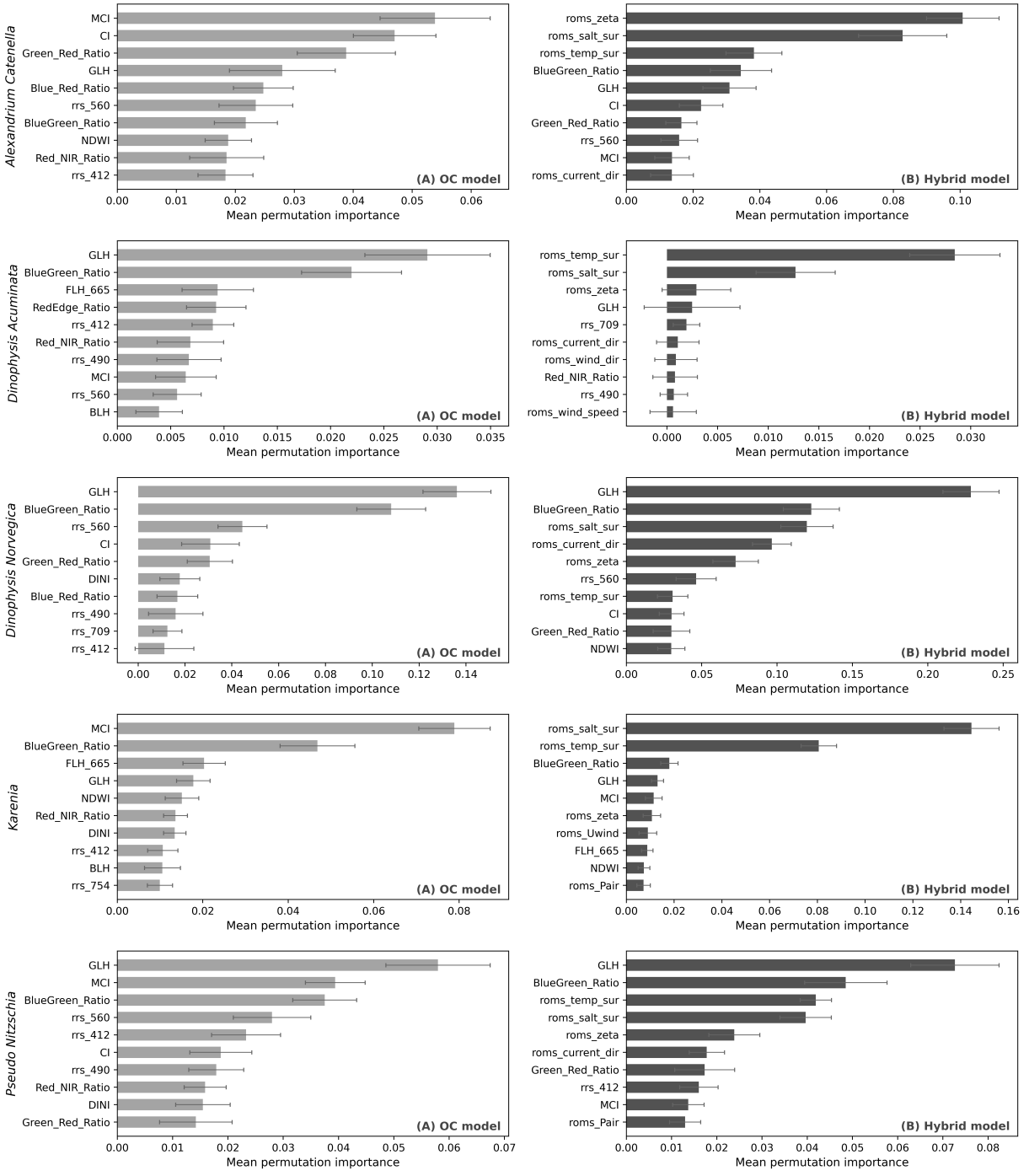


**Figure A.6: Top 10 permutation-importance per species for ACOLITE at the warning threshold**. Error bars indicate ± one standard deviation. Plots in each row indicate permutation importance for specific taxa. Left column represents (A) Ocean color model; and right column plots indicate (B) Hybrid model (ocean color + ROMS features).

## References


Alvarez, S., Brown, C.E., Garcia Diaz, M., O'Leary, H., Solís, D., 2024. Non-linear impacts of harmful algae blooms on the coastal tourism economy. Journal of Environmental Management 351, 119811. doi:10.1016/j.jenvman.2023.119811.

Amin, R., Zhou, J., Gilerson, A., Gross, B., Moshary, F., Ahmed, S., 2009. Novel optical techniques for detecting and classifying toxic dinoflagellate Karenia brevis blooms using satellite imagery. Optics Express 17, 9126–9144. doi:10.1364/OE.17.009126.

Anderson, C.R., Berdalet, E., Kudela, R.M., Cusack, C.K., Silke, J., O'Rourke, E., Dugan, D., McCammon, M., Newton, J.A., Moore, S.K., Paige, K., Ruberg, S., Morrison, J.R., Kirkpatrick, B., Hubbard, K., Morell, J., 2019. Scaling Up From Regional Case Studies to a Global Harmful Algal Bloom Observing System. Frontiers in Marine Science 6. doi:10.3389/fmars.2019.00250.

Anderson, D.M., Fensin, E., Gobler, C.J., Hoeglund, A.E., Hubbard, K.A., Kulis, D.M., Landsberg, J.H., Lefebvre, K.A., Provoost, P., Richlen, M.L., Smith, J.L., Solow, A.R., Trainer, V.L., 2021. Marine harmful algal blooms (HABs) in the United States: History, current status and future trends. Harmful Algae 102, 101975. doi:10.1016/j.hal.2021.101975.

Anderson, D.M., Keafer, B.A., Kleindinst, J.L., McGillicuddy, D.J., Martin, J.L., Norton, K., Pilskaln, C.H., Smith, J.L., Sherwood, C.R., Butman, B., 2014. Alexandrium fundyense cysts in the Gulf of Maine: Long-term time series of abundance and distribution, and linkages to past and future blooms. Deep-sea research. Part II, Topical studies in oceanography 103, 6–26. doi:10.1016/j.dsr2.2013.10.002.

Baek, S.S., Kwon, Y.S., Pyo, J., Choi, J., Kim, Y.O., Cho, K.H., 2021. Identification of influencing factors of *A. catenella* bloom using machine learning and numerical simulation. Harmful Algae 103, 102007. doi:10.1016/j.hal.2021.102007.

Blanco, J.C., Reguera, B., 2019. Dinophysis Toxins: Distribution, Fate in Shellfish and Impacts. MDPI - Multidisciplinary Digital Publishing Institute, Erscheinungsort nicht ermittelbar.

Breiman, L., 2001. Random Forests. Machine Learning 45, 5–32. doi:10.1023/A:1010933404324.

Brockmann, C., Doerffer, R., Peters, M., Kerstin, S., Embacher, S., Ruescas, A., 2016. Evolution of the c2rcc neural network for sentinel 2 and 3 for the retrieval of ocean colour products in normal and extreme optically complex waters, in: Living planet symposium, p. 54.

Carias, J., Vásquez-Lavín, F., Barrientos, M., Ponce Oliva, R.D., Gelcich, S., 2024. Economic valuation of Harmful Algal Blooms (HAB): Methodological challenges, policy implications, and an empirical application. Journal of Environmental Management 365, 121566. doi:10.1016/j.jenvman.2024.121566.

Chen, S., Chen, X., Peng, Y., Peng, K., 2009. A mathematical model of the effect of nitrogen and phosphorus on the growth of blue-green algae population. Applied Mathematical Modelling 33, 1097–1106. URL: https://www.sciencedirect.com/science/article/pii/S0307904X08000024, doi:10.1016/j.apm.2008.01.001.

for Copernicus, E., 2022. Olci level 2 ocean colour full resolution (version bc003) - sentinel-3 - reprocessed. URL: https://user.eumetsat.int/catalogue/EO:EUM:DAT:0556, doi:10.15770/EUM_SEC_CLM_0061.

Cruz, R.C., Reis Costa, P., Vinga, S., Krippahl, L., Lopes, M.B., 2021. A Review of Recent Machine Learning Advances for Forecasting Harmful Algal Blooms and Shellfish Contamination. Journal of Marine Science and Engineering 9, 283. doi:10.3390/jmse9030283.

D. Kovács, D., Musial, J., Bojanowski, J., Clarijs, D., de la Mar, J., Zlinszky, A., 2026. Copernicus Data Space Ecosystem establishes public cloud processing for earth observation data. Scientific Data 13, 537. doi:10.1038/s41597-026-06765-8.

Davis, J., Goadrich, M., 2006. The relationship between Precision-Recall and ROC curves, in: Proceedings of the 23rd International Conference on Machine Learning, Association for Computing Machinery, New York, NY, USA. pp. 233–240. doi:10.1145/1143844.1143874.

Doerffer, R., Schiller, H., 2007. The MERIS Case 2 water algorithm. International Journal of Remote Sensing 28, 517–535. doi:10.1080/01431160600821127.

Donlon, C., Berruti, B., Buongiorno, A., Ferreira, M.H., Féménias, P., Frerick, J., Goryl, P., Klein, U., Laur, H., Mavrocordatos, C., Nieke, J., Rebhan, H., Seitz, B., Stroede, J., Sciarra, R., 2012. The Global Monitoring for Environment and Security (GMES) Sentinel-3 mission. Remote Sensing of Environment 120, 37–57. doi:10.1016/j.rse.2011.07.024.

European Space Agency, 2025. Snap (sentinel application platform). https://step.esa.int/main/download/snap-download. Version 12.0.0, released 08 May 2025.

Gobler, C.J., Doherty, O.M., Hattenrath-Lehmann, T.K., Griffith, A.W., Kang, Y., Litaker, R.W., 2017. Ocean warming since 1982 has expanded the niche of toxic algal blooms in the North Atlantic and North Pacific oceans. Proceedings of the National Academy of Sciences 114, 4975–4980. doi:10.1073/pnas.1619575114.

Gower, J., King, S., Borstad, G., Brown, L., 2005. Detection of intense plankton blooms using the 709 nm band of the MERIS imaging spectrometer. International Journal of Remote Sensing 26, 2005–2012. doi:10.1080/01431160500075857.

Gower, J., King, S., Goncalves, P., 2008. Global monitoring of plankton blooms using MERIS MCI. International Journal of Remote Sensing 29, 6209–6216. doi:10.1080/01431160802178110.

Hallegraeff, G.M., Anderson, D.M., Belin, C., Bottein, M.Y.D., Bresnan, E., Chinain, M., Enevoldsen, H., Iwataki, M., Karlson, B., McKenzie, C.H., Sunesen, I., Pitcher, G.C., Provoost, P., Richardson, A., Schweibold, L., Tester, P.A., Trainer, V.L., Yñiguez, A.T., Zingone, A., 2021. Perceived global increase in algal blooms is attributable to intensified monitoring and emerging bloom impacts. Communications Earth & Environment 2, 117. doi:10.1038/s43247-021-00178-8.

Harley, J.R., Lanphier, K., Kennedy, E., Whitehead, C., Bidlack, A., 2020. Random forest classification to determine environmental drivers and forecast paralytic shellfish toxins in Southeast Alaska with high temporal resolution. Harmful Algae 99, 101918. doi:10.1016/j.hal.2020.101918.

Hattenrath-Lehmann, T.K., Marcoval, M.A., Berry, D.L., Fire, S., Wang, Z., Morton, S.L., Gobler, C.J., 2013. The emergence of *Dinophysis acuminata* blooms and DSP toxins in shellfish in New York waters. Harmful Algae 26, 33–44. doi:10.1016/j.hal.2013.03.005.

He, R., McGillicuddy Jr., D.J., Keafer, B.A., Anderson, D.M., 2008. Historic 2005 toxic bloom of Alexandrium fundyense in the western Gulf of Maine: 2. Coupled biophysical numerical modeling. Journal of Geophysical Research: Oceans 113. doi:10.1029/2007JC004602.

Hetland, R.D., Signell, R.P., 2005. Modeling coastal current transport in the Gulf of Maine. Deep Sea Research Part II: Topical Studies in Oceanography 52, 2430–2449. doi:10.1016/j.dsr2.2005.06.024.

Hoagland, P., Anderson, D.M., Kaoru, Y., White, A.W., 2002. The Economic Effects of Harmful Algal Blooms in the United States: Estimates, Assessment Issues, and Information Needs. Estuaries 25, 819–837. doi:10.1007/BF02804908, arXiv:1353035.

Hoagland, P., Scatasta, S., 2006. The Economic Effects of Harmful Algal Blooms, in: Ecology of Harmful Algae. Ecology Studies Series. volume 189, pp. 391–402. doi:10.1007/978-3-540-32210-8_30.

Hu, C., Muller-Karger, F.E., Taylor, C.J., Carder, K.L., Kelble, C., Johns, E., Heil, C.A., 2005. Red tide detection and tracing using MODIS fluorescence data: A regional example in SW Florida coastal waters. Remote Sensing of Environment 97, 311–321. doi:10.1016/j.rse.2005.05.013.

Izadi, M., Sultan, M., Kadiri, R.E., Ghannadi, A., Abdelmohsen, K., 2021. A Remote Sensing and Machine Learning-Based Approach to Forecast the Onset of Harmful Algal Bloom. Remote Sensing 13, 3863. doi:10.3390/rs13193863.

Jin, D., Wang, A., Dalton, T., 2025. Economic impacts of sargassum events in Puerto Rico, USVI, and coastal Florida. Harmful Algae 150, 102996. doi:10.1016/j.hal.2025.102996.

Kapoor, S., Narayanan, A., 2023. Leakage and the reproducibility crisis in machine-learning-based science. Patterns 4, 100804. doi:10.1016/j.patter.2023.100804.

Kudela, R.M., Palacios, S.L., Austerberry, D.C., Accorsi, E.K., Guild, L.S., Torres-Perez, J., 2015. Application of hyperspectral remote sensing to cyanobacterial blooms in inland waters. Remote Sensing of Environment 167, 196–205. doi:10.1016/j.rse.2015.01.025.

Lange, P.K., Fachon, E., Nielsen, J.M., Brosnahan, M., Zhang, J., Mordy, C.W., Gann, J.C., Lomas, M.W., Pate, E., Sheffield, G., Stabeno, P., Robinson, D., Pathare, M., Lefebvre, K.A., Anderson, D.M., Eisner, L.B., 2025. Application of dinoflagellate-specific satellite models to aid *Alexandrium catenella* bloom monitoring in the Bering and Chukchi seas. Journal of Environmental Management 380, 125042. doi:10.1016/j.jenvman.2025.125042.

Li, Y., Stumpf, R.P., McGillicuddy, D.J., He, R., 2020. Dynamics of an intense *Alexandrium catenella* red tide in the Gulf of Maine: Satellite observations and numerical modeling. Harmful Algae 99, 101927. doi:10.1016/j.hal.2020.101927.

Manning, C.D., Raghavan, P., Schütze, H., 2008. Introduction to Information Retrieval. Cambridge University Press, USA.

McFEETERS, S.K., 1996. The use of the Normalized Difference Water Index (NDWI) in the delineation of open water features. International Journal of Remote Sensing 17, 1425–1432. doi:10.1080/01431169608948714.

McGillicuddy, D. J., Jr., Townsend, D.W., He, R., Keafer, B.A., Kleindinst, J.L., Li, Y., Manning, J.P., Mountain, D.G., Thomas, M.A., Anderson, D.M., 2011. Suppression of the 2010 Alexandrium fundyense bloom by changes in physical, biological, and chemical properties of the Gulf of Maine. Limnology and Oceanography 56, 2411–2426. doi:10.4319/lo.2011.56.6.2411.

Medina, M., Julian, P., Chin, N., Davis, S.E., 2024. An early-warning forecast model for red tide (*Karenia brevis*) blooms on the southwest coast of Florida. Harmful Algae 139, 102729. doi:10.1016/j.hal.2024.102729.

Mishra, S., Mishra, D.R., 2012. Normalized difference chlorophyll index: A novel model for remote estimation of chlorophyll-*a* concentration in turbid productive waters. Remote Sensing of Environment 117, 394–406. doi:10.1016/j.rse.2011.10.016.

Mobley, C.D., 1994. Light and Water : Radiative Transfer in Natural Waters. San Diego : Academic Press.

Olson, R., Sosik, H., 2007. A submersible imaging-in-flow instrument to analyze nano- and microplankton: Imaging FlowCytobot. Limnology and Oceanography: Methods 5, 195–203. doi:10.4319/lom.2007.5.195.

Park, J., Patel, K., Lee, W.H., 2024. Recent advances in algal bloom detection and prediction technology using machine learning. Science of The Total Environment 938, 173546. doi:10.1016/j.scitotenv.2024.173546.

Pershing, A.J., Alexander, M.A., Hernandez, C.M., Kerr, L.A., Le Bris, A., Mills, K.E., Nye, J.A., Record, N.R., Scannell, H.A., Scott, J.D., Sherwood, G.D., Thomas, A.C., 2015. Slow adaptation in the face of rapid warming leads to collapse of the Gulf of Maine cod fishery. Science 350, 809–812. doi:10.1126/science.aac9819.

Record, N.R., Countway, P.D., Kanwit, K., Fernández-Robledo, J.A., 2021. Rise of the rare biosphere: Thinking beyond climate envelopes for forecasting harmful algal blooms. Elementa: Science of the Anthropocene 9, 00056. doi:10.1525/elementa.2020.00056.

Reguera, B., Riobó, P., Rodríguez, F., Díaz, P.A., Pizarro, G., Paz, B., Franco, J.M., Blanco, J., 2014. Dinophysis Toxins: Causative Organisms, Distribution and Fate in Shellfish. Marine Drugs 12, 394–461. doi:10.3390/md12010394.

Saito, T., Rehmsmeier, M., 2015. The precision-recall plot is more informative than the ROC plot when evaluating binary classifiers on imbalanced datasets. PloS One 10, e0118432. doi:10.1371/journal.pone.0118432.

Shchepetkin, A.F., McWilliams, J.C., 2005. The regional oceanic modeling system (ROMS): A split-explicit, free-surface, topography-following-coordinate oceanic model. Ocean Modelling 9, 347–404. doi:10.1016/j.ocemod.2004.08.002.

solvo, HYGEOS, 2023. Ocean Colour Standard Atmospheric Correction (OC-SAC) Algorithm Theoretical Basis Document (ATBD). Technical Report EUM/21/SAC/ATBD. EUMETSAT. URL: https://user.eumetsat.int/s3/ope-eup-strapi-media/S3_OLCI_OC_Standard_Atmospheric_Correction_ATBD_df315c5f8a.pdf.

Sosik, H.M., Olson, R.J., 2007. Automated taxonomic classification of phytoplankton sampled with imaging-in-flow cytometry. Limnology and Oceanography: Methods 5, 204–216. URL: https://aslopubs.onlinelibrary.wiley.com/doi/abs/10.4319/lom.2007.5.204, doi:https://doi.org/10.4319/lom.2007.5.204, arXiv:https://aslopubs.onlinelibrary.wiley.com/doi/pdf/10.4319/lom.2007.5.204.

Sosik, H.M., Peacock, E., Santos, M., 2020. Abundance and biovolume of taxonomically-resolved phytoplankton and microzooplankton imaged continuously underway with an Imaging FlowCytobot along the NES-LTER Transect in winter 2018. doi:10.6073/PASTA/74775C4AF51C237F2A20E4A8C011BC53.

Stumpf, R.P., Culver, M.E., Tester, P.A., Tomlinson, M., Kirkpatrick, G.J., Pederson, B.A., Truby, E., Ransibrahmanakul, V., Soracco, M., 2003. Monitoring *Karenia brevis* blooms in the Gulf of Mexico using satellite ocean color imagery and other data. Harmful Algae 2, 147–160. doi:10.1016/S1568-9883(02)00083-5.

Stumpf, R.P., Li, Y., Kirkpatrick, B., Litaker, R.W., Hubbard, K.A., Currier, R.D., Harrison, K.K., Tomlinson, M.C., 2022. Quantifying Karenia brevis bloom severity and respiratory irritation impact along the shoreline of Southwest Florida. PLOS ONE 17, e0260755. doi:10.1371/journal.pone.0260755.

Suddleson, M., Hoagland, P., 2021. Proceedings of the Workshop on the Socio-economic Effects of Harmful Algal Blooms in the United States. https://repository.library.noaa.gov.

Tamvakis, A., Tsirtsis, G., Karydis, M., Patsidis, K., Kokkoris, G.D., Tamvakis, A., Tsirtsis, G., Karydis, M., Patsidis, K., Kokkoris, G.D., 2021. Drivers of harmful algal blooms in coastal areas of Eastern Mediterranean: A machine learning methodological approach. Mathematical Biosciences and Engineering 18, 6484–6505. doi:10.3934/mbe.2021322.

Tomlinson, M.C., Wynne, T.T., Stumpf, R.P., 2009. An evaluation of remote sensing techniques for enhanced detection of the toxic dinoflagellate, *Karenia brevis*. Remote Sensing of Environment 113, 598–609. doi:10.1016/j.rse.2008.11.003.

Townhill, B.L., Tinker, J., Jones, M., Pitois, S., Creach, V., Simpson, S.D., Dye, S., Bear, E., Pinnegar, J.K., 2018. Harmful algal blooms and climate change: Exploring future distribution changes. ICES Journal of Marine Science 75, 1882–1893. doi:10.1093/icesjms/fsy113.

Townsend, D., Rebuck, N., Thomas, M., Karp-Boss, L., Gettings, R., 2010. A changing nutrient regime in the Gulf of Maine. Continental Shelf Research - CONT SHELF RES 30, 820–832. doi:10.1016/j.csr.2010.01.019.

Townsend, D., THOMAS, A., MAYER, L., THOMAS, M., Quinlan, J., 2006. Oceanography of the northwest Atlantic continental shelf (1, W). The Sea: The Global Coastal Ocean 144.

Trainer, V.L., Bates, S.S., Lundholm, N., Thessen, A.E., Cochlan, W.P., Adams, N.G., Trick, C.G., 2012. *Pseudo-Nitzschia* physiological ecology, phylogeny, toxicity, monitoring and impacts on ecosystem health. Harmful Algae 14, 271–300. doi:10.1016/j.hal.2011.10.025.

Trainer, V.L., Moore, S.K., Hallegraeff, G., Kudela, R.M., Clement, A., Mardones, J.I., Cochlan, W.P., 2020. Pelagic harmful algal blooms and climate change: Lessons from nature's experiments with extremes. Harmful Algae 91, 101591. doi:10.1016/j.hal.2019.03.009.

Trainer, V.L., Suddleson, M., 2005. Monitoring approaches for early warning of domoic acid events in washington state. Oceanography 18, 228–237.

Vanhellemont, Q., Ruddick, K., 2021. Atmospheric correction of Sentinel-3/OLCI data for mapping of suspended particulate matter and chlorophyll-a concentration in Belgian turbid coastal waters. Remote Sensing of Environment 256, 112284. doi:10.1016/j.rse.2021.112284.

Weir, M.J., Kourantidou, M., Jin, D., 2022. Economic impacts of harmful algal blooms on fishery-dependent communities. Harmful Algae 118, 102321. doi:10.1016/j.hal.2022.102321.

Yang, Z., Richardson, P., Chen, Y., Myers, E.P., Aikman, F., Kelley, J.G.W., Peng, M., Zhang, A., 2019. NOAA's Gulf of Maine Operational Forecast System (GOMOFS): Model Development and Hindcast Skill Assessment. https://repository.library.noaa.gov. URL: https://repository.library.noaa.gov, doi:10.25923/0m2e-xg81.